Sensitivity of Model Simulations for a Coastal Cyclone

ISIDORO ORLANSKI AND JACK J. KATZFEY

Geophysical Fluid Dynamics Laboratory/NOAA, Princeton University, Princeton, NJ 08542

(Manuscript received 30 May 1986, in final form 15 May 1987)

ABSTRACT

A nested global, limited-area model was used to predict the Presidents' Day cyclone of 18–19 February 1979. Both a low (~150 km) and a high (~50 km) horizontal resolution version were used. The model has full physics with a planetary boundary layer, moisture, moist convective adjustment, and radiation.

The low-resolution model, using a global analysis for initial and boundary conditions (termed a simulation), was able to capture the general development and movement of the cyclone. Some discrepancies were noted for the intensity of upper-air features between the analyses and the model solution during the first 24 hours. The primary focus of this paper is to determine the effect of initial and boundary conditions, as well as model parameterizations on the accuracy of the predictions. The evolution of the storm is discussed with an emphasis on the quality of the numerical simulation.

The impact of the initial conditions on the model solution was tested by using four different global analyses. It was found that the variability between the solutions was less than the variability between the analyses. Varying the horizontal diffusion in the model produced stronger development with weaker diffusion, but the character of the development did not change significantly. The sensitivity of the simulation to latent heat was tested by running the model without latent heating. A low did develop in this model solution, although it was much weaker and it did not develop vertically as in the cases with latent heating.

The most significant improvement in accuracy in this sensitivity study occurred when the horizontal resolution was increased from 1.25° × 1.0° (~150 km) to 0.4° × 0.32° (~50 km). The position and intensity of the surface low were much closer to reality, as indicated by comparison with a mesoanalysis and to satellite pictures.

The nested model was also run in forecast mode with boundary conditions for the limited-area model supplied by the (Geophysical Fluid Dynamics Laboratory) GFDL global spectral model forecast. In general, the quality of the limited-area forecast compared very well with the simulations. The overall character and intensity of the development were similar.

The role of lateral boundary conditions was demonstrated by comparing forecasts and simulations with identical initial conditions. The results suggest the increasing importance of the boundary data with time in the limited-area forecast and show high correlation between the errors in the limited-area forecast and the global forecast within the limited-area domain.

1. Introduction

Considerable improvements have been obtained in simulating meso-alpha phenomena (200–2000 km) in the last five years using sophisticated limited-area models. In a number of studies based on numerical simulations of mesoscale systems, suggestions have been offered on the mechanisms responsible for the occurrence of significant weather phenomena. Some recent examples include the dynamics of hurricanes upon landfall (Tuleya et al., 1984), the processes important for maintaining a mature cold front (Orlanski et al., 1985), the relative importance of the wind field for convective storms (Anthes et al., 1982; Weisman and Klemp, 1982) and the important role of surface convergence in forcing squall lines (Ross, 1987). These and other studies have improved our knowledge of the prestorm environment.

Better numerical simulations of mesoconvective systems have resulted from more sophisticated physics in the numerical models, more computer power that permits higher model resolution, mesoscale field experiments like SESAME[1] and ALPEX[2], and better data analyses for model initialization and verification. However, despite the advancement in mesoscale research, the improvements in short-range forecasting (6–48 h) are not nearly as impressive. Multiple reasons have been given for this performance including poor initialization, coarse model resolution and lack of sophisticated physics (Anthes, 1983). It is important to recognize that the requirements for an accurate operational forecast are more stringent than for numerical simulations used for research. The simulation is considered satisfactory in a research mode when the numerical solution captures the dynamics and thermodynamics of the simulated phenomena, whereas the precise geographical location of the storm is not as im-

[1] Severe Environmental Storms And Mesoscale Experiment.
[2] ALPine EXperiment.

portant for the understanding of the processes involved. In a forecast mode, however, the proper location and intensity of the storm is of crucial importance.

Mesoscale weather phenomena can be classified in two major categories: (i) ones that are generated, triggered or strongly influenced by local forcing, such as orography, surface sensible and/or latent heating, roughness, etc., and (ii) those generated by instabilities or the nonlinear evolution of the planetary-scale environment; for example, baroclinicity, advection of heat and moisture, jet streaks, etc.

In a recent study, Orlanski et al. [1983, hereafter referred to as OMM; see Orlanski (1984) for more detail] have pointed out that the accuracy of a forecast with a limited-area model depends not only on the quality of the model and the initial data, but also in large part on the quality of the coarser model forecast that provides the information to the boundaries of the nested model.

The study of OMM has shown that, for the forecast of mesoscale phenomena of type (ii), the position of the planetary baroclinic wave is of paramount importance in determining the position of the cold front in the fine-resolution limited-area model. The evolution of the large-scale baroclinic wave is controlled by the coarse global model (a spectral model was used in that experiment) which provided the information to the boundaries of the limited-area model continuously over the period of integration (48 h). The position of the baroclinic wave itself will have the accuracy of the coarser global model, say a few grid increments (at least $2\Delta X$) of this model. Regardless of how well the fine-resolution model is performing in accurately generating the intensity of the front, the position of the front will be determined by the larger-scale wave and will be displaced by the same $2\Delta X$ of the coarse model.

Basically, the problem reduces to determining the time period over which errors from the "outside influence" will contaminate the limited-area solution. For instance, the position of a hurricane could be accurately forecasted for a period of 24 hours with a high-resolution nested system, but the skill of a longer forecast would depend on the skill of the forecast of the planetary scales that influence the hurricane. This is in accordance with the results of Koch et al. (1985), where the primary source of errors for the synoptic scale was found to be associated with errors in the lateral boundary conditions of the model. There is some indication from unpublished skill scores that the skill of forecasts may show better performance of limited-area models than the global forecast for 24 hours but nearly the same skill for 48 hours.

In general, the operational models accurately predict cyclogenesis within the conterminous United States. However, in an exceptional case, the operational Limited Fine-Mesh model failed to predict the rapid cyclogenesis that occurred along the Atlantic coast on 18–19 February 1979, called the "Presidents' Day Cyclone." Bosart (1981) concluded that possible reasons for this failure are "inadequate vertical resolution, omission of significant-level sounding data from the initial analysis cycle, improper boundary layer physics, and the inability to simulate the bulk effects of convective processes adequately" (Bosart, 1981, p. 1564). Although all these reasons can cause bad forecasts, it is important to quantitatively isolate reasons why a limited-area model fails to predict these severe conditions.

The purpose of this paper is to evaluate the sensitivity of a model solution with a one-way nested system (similar to that used by OMM) to different parameters that may affect the forecast: the quality of the initial condition, subgrid-scale parameterization, horizontal resolution and the outside influence. The storm chosen for this study is the snowstorm of 18–19 February 1979, which developed along the east coast of the U.S. and left up to 60 cm of snow over Virginia, Maryland and Delaware. Observational studies of this storm have emphasized both the local forcing (Bosart, 1981; Bosart and Lin, 1984) and the larger-scale forcing (Uccellini et al., 1984, 1985). Thus, this case of cyclogenesis has many of the features noted earlier. Since this study intends to investigate the sensitivity of the limited-area model for this case and for a straightforward comparison with other operational and forecast experiments (including global forecasts), the standard sea level pressure, 500 mb geopotentials, and 500 mb relative vorticity fields will be the primary fields shown. A more detailed look at the various mesoscale features of this storm noted by previous investigators will be analyzed elsewhere.

2. Observed conditions

The development of the Presidents' Day cyclone is described in this section using the standard GFDL/FGGE[3] archived analysis. A description of the GFDL four-dimensional analysis scheme is given in Stern and Ploshay (1983). The FGGE analysis is one of the more complete sets of global analyses from which a global forecast can be made. It includes buoys, ships, and other nonstandard observations, as well as the standard radiosonde network in the analysis. Since the nested system uses either a global analysis or a global spectral forecast for boundary conditions for the limited-area model, this analysis is a natural choice to document the improvements in the limited-area model. The approximate grid spacing of the GFDL/FGGE analysis is 3° (~300 km).

The GFDL/FGGE analysis of sea level pressure for every 12 hours from 0000 UTC 19 to 1200 UTC 20 February 1979 is shown in Fig. 1. A more detailed

[3] First GARP (Global Atmospheric Research Program) Global Experiment.

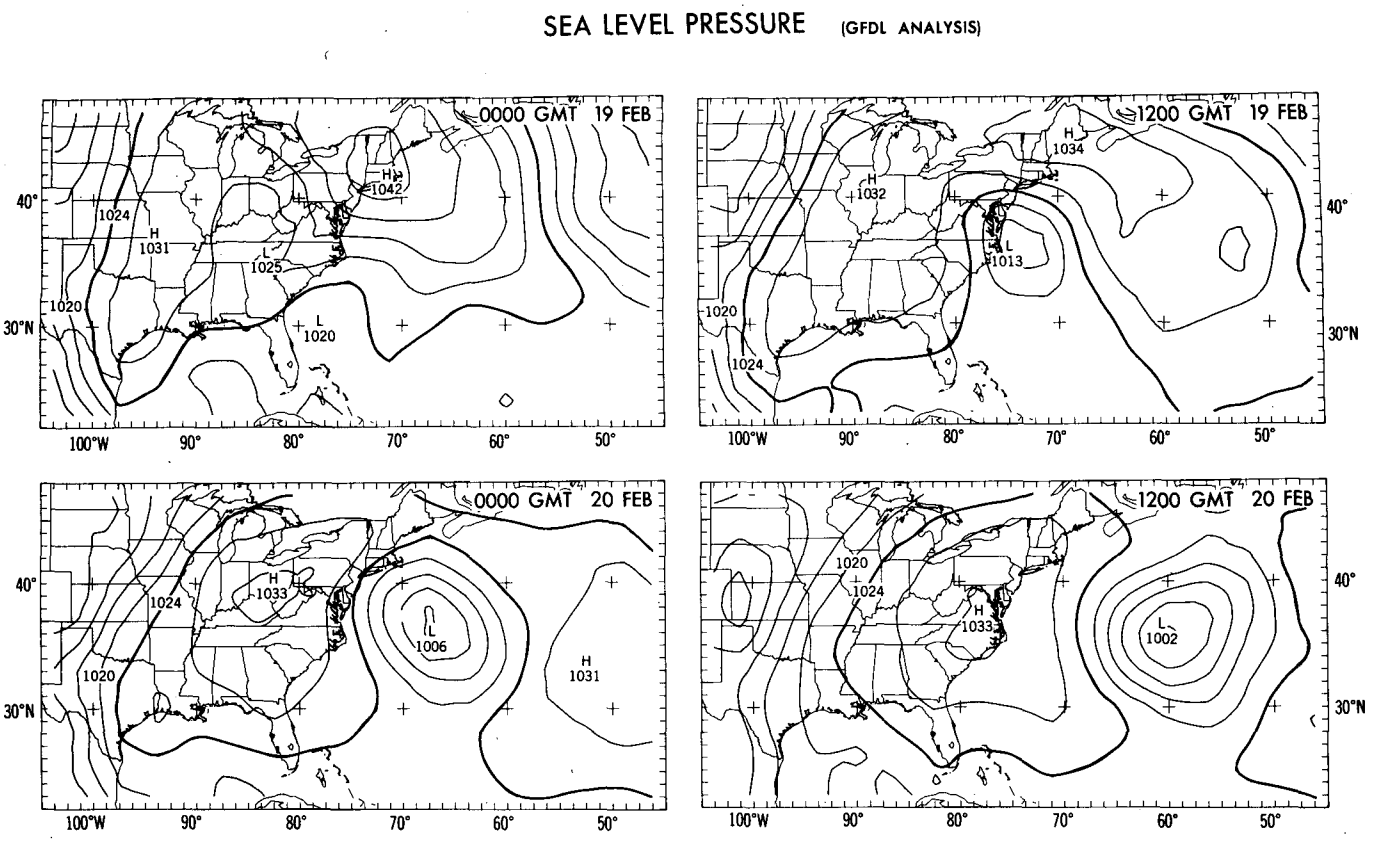

FIG. 1. Sea level pressure in millibars from GFDL analysis for period 0000 UTC 19–1200 UTC 20 February 1979. Contour interval = 4 mb with 1024 mb contour darkened.

analysis of the sea level pressure field is presented in Bosart (1981). Initially a large anticyclone (1042 mb) was located over New England. The developing low (1020 mb) had just formed off the coast of Florida with an inverted trough extending along the coast. Another inverted trough was evident over the Ohio Valley.

During the next 12 hours, the low deepened to 1013 mb and moved northeastward along the coast to a position just off the North Carolina coast at 1200 UTC 19 February. The inverted trough that was over Ohio was no longer evident. The high pressure over New England had weakened to 1034 mb and had shifted northeastward.

The low moved eastward and continued to intensify during the next 12 hours to 1006 mb in the GFDL/FGGE analysis by 0000 UTC 20 February. The high over New England had split, with one center located east of the low (1031 mb) and the other located over the Ohio Valley (1033 mb).

By 1200 UTC 20 February, the low had continued to translate eastward and had deepened to 1002 mb in the GFDL/FGGE analysis. The main high was located over North Carolina, with a central pressure of 1033 mb.

The 500 mb geopotential heights for the same four time periods are presented in Fig. 2. The short-wave trough, located over Illinois and Indiana at 0000 UTC 19 February, was related to the inverted trough at the surface noted previously. No upper-level disturbance is evident above the developing surface low in the geopotential at this level.

During the next 12 hours, the 500 mb short wave propagated eastward and approached the surface low at 1200 UTC 19 February. Ridging was evident east of the short wave just off the east coast. At 0000 UTC 20 February, the short wave in the height field becomes broader while ridging is observed over the Ohio Valley. The short wave apparently deepens again by 1200 UTC 20 February.

The relative vorticity at 500 mb for the same four time periods is shown in Fig. 3. The short wave over Illinois is clearly evident at 0000 UTC 19 February, with a maximum of 95×10^{-6} s^{-1}. A departing trough is indicated over the northeast portion of the domain. The negative relative vorticities in the southeastern portion of the domain (up to -103×10^{-6} s^{-1}) seem unrealistically large.

The vorticity of the short wave increased in the analysis during the 12 hours ending 1200 UTC 19 February with the maximum of 129×10^{-6} s^{-1}. The trough in the northeast and the larger negative relative vorticities in the southeast have decreased and moved out of the

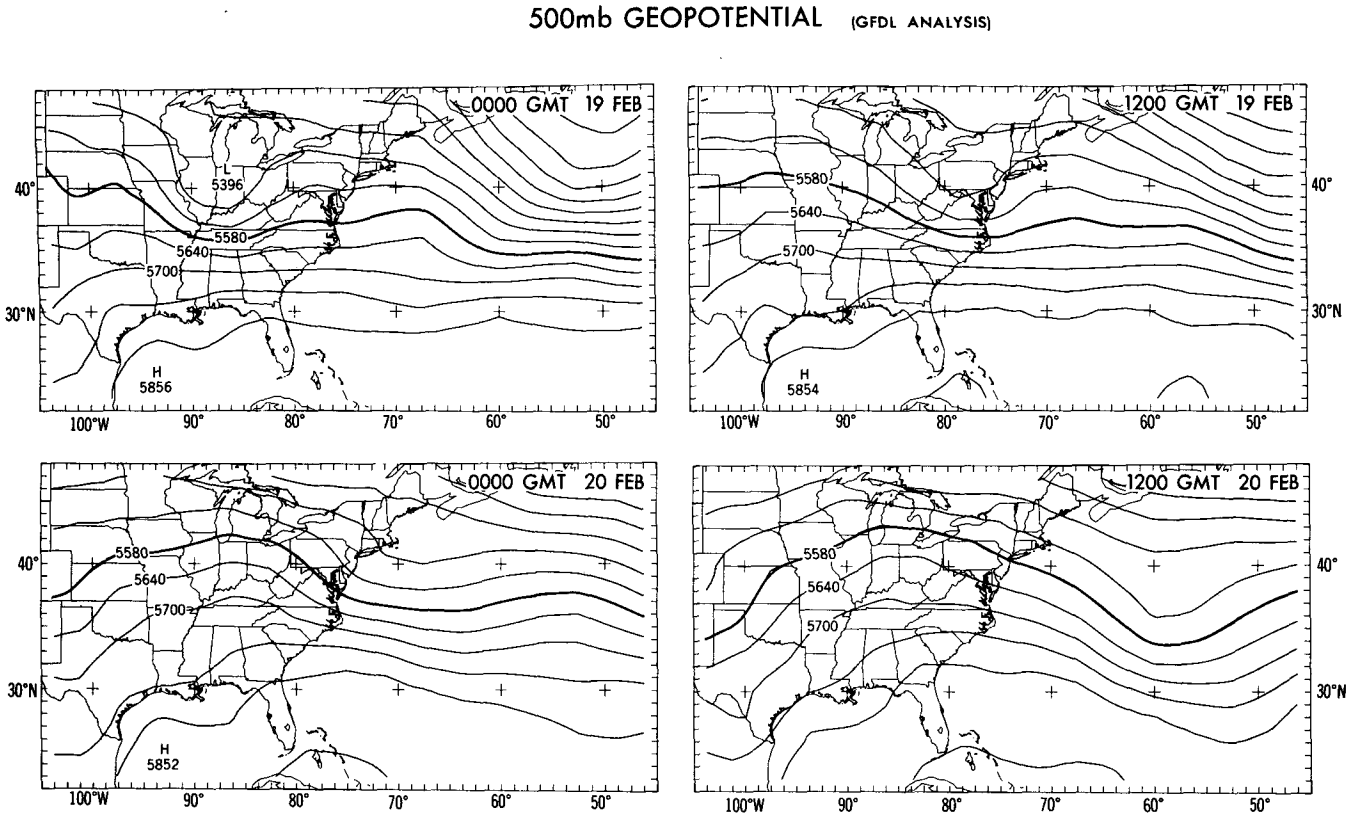

FIG. 2. 500 mb geopotential heights in meters from GFDL analysis for same times as Fig. 1. Contour interval = 60 m with 5580 m contour darkened.

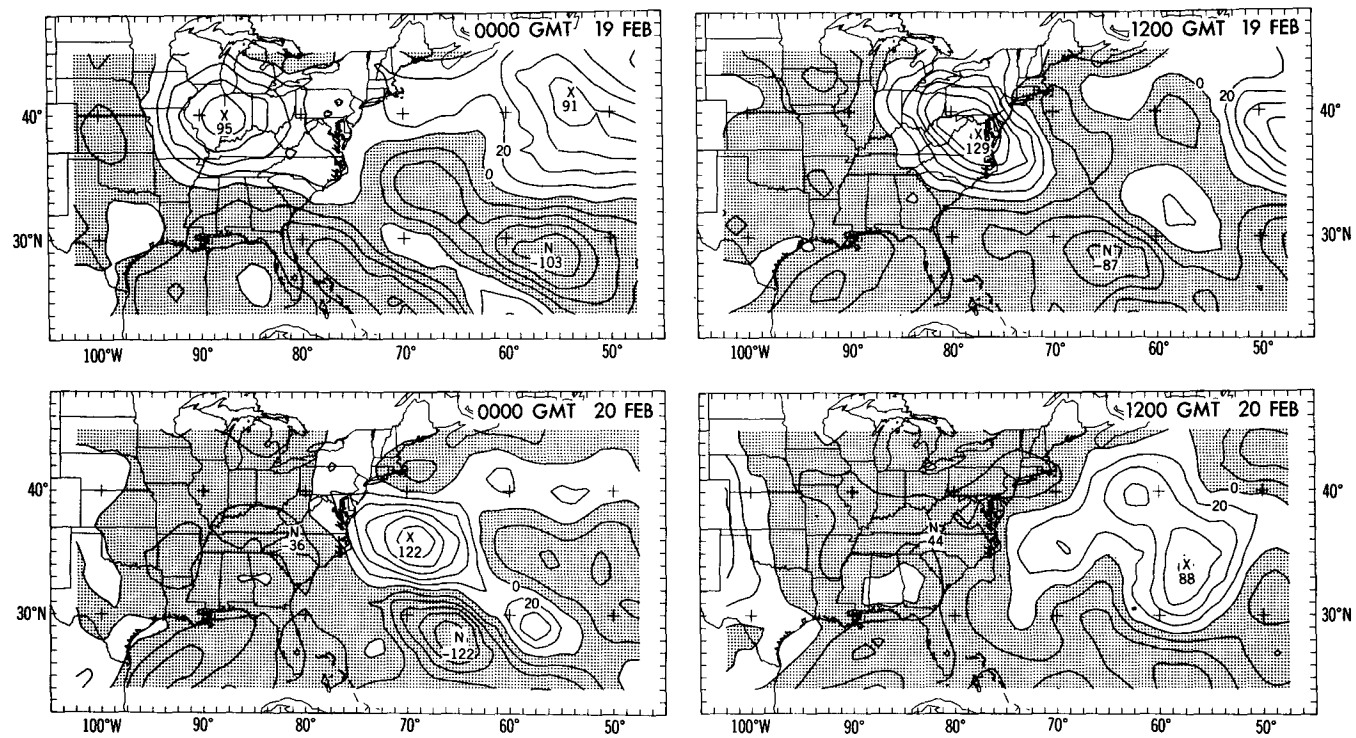

FIG. 3. Vertical component of 500 mb relative vorticity (10^{-6} s^{-1}) from GFDL analysis for same times as Fig. 1. Contour interval = 20×10^{-6} s^{-1} with negative values shaded.

domain. Some negative vorticities, associated with ridging over the Mississippi, are evident.

The intensity of the short-wave vorticity remained fairly constant during the next 12 hours, with a maximum of 122×10^{-6} s^{-1} at 0000 UTC 20 February. This is an apparent discrepancy, since the trough in the geopotential was weaker than 12 hours previously. Negative relative vorticities south of the short wave have increased to -122×10^{-6} s^{-1} at this time. The ridging over the Mississippi Valley associated with negative vorticities is still evident.

By 1200 UTC 20 February, there has been a significant decrease of the vorticity maximum associated with the short wave in the analysis, with a maximum of only 88×10^{-6} s^{-1}. In addition, a less-coherent distribution of vorticity in the analysis is associated with the short wave. Again, this contrasts with the geopotential, which appeared to be deeper. The large negative vorticities, located south of the short wave, have decreased in magnitude. Negative vorticity associated with ridging is evident over the eastern United States, while positive relative vorticities along the western edge of the domain are indicative of an approaching trough.

The lack of coherence of some features in this analysis and the lack of intensity of the surface wave indicate that this analysis has some problems not solely attributable to lack of resolution. This points out that regional studies like this can find possible inconsistencies in global analyses which global averages or mean statistics may not capture. The GFDL/FGGE analysis is being redone for the special observing periods during FGGE in order to improve the analysis (Stern and Ploshay, 1987). Preliminary results shows significant improvement of the new analysis over the one used in this study.

3. Model description

The nested global, limited-area system used in this study is the same one used in OMM and Orlanski (1984). A complete description of models used is given in the Appendix. A discussion of the relevant features for the two modes in which the model was run are subsequently discussed.

The lateral boundary conditions can be derived from two sources. First, global analyses every 12 hours can be interpolated to the boundary of the limited-area domain. The boundary conditions for the limited-area model are then linearly interpolated temporally between analysis times. The limited-area model using these boundary conditions will be termed a "simulation", since observed conditions are used at the boundaries.

An alternative source for boundary condition data can be from a global model forecast. The boundary condition for the limited-area model is continually fed from a version of the GFDL spectral model of Gordon and Stern (1982), with nine sigma levels and rhomboidal truncation of the spherical harmonic fields at wavenumber 30 (R30L9). This limited-area model is termed a "forecast", since it uses data based on observations only at the initial time period.

The boundary conditions are explicitly determined at the outer boundary of the limited-area model by one of the above modes. Averaging of the internal grid points and boundary data is done at the next (inner) set of grid points. Finally, in the border region a Lagrangian-type upstream advection is used with the horizontal diffusion coefficient set to a value larger than in the interior of the grid.

The impact of the initial analysis on the limited-area simulation will be discussed in the next section. This is accomplished through use of the GFDL, ECMWF, NMC, and GLAS analyses to initialize the model. The simulation using the GFDL analysis is the control simulation of this study and is discussed first.

4. GFDL/FGGE control simulation

Sensitivity of the simulation to different model parameters can be evaluated more precisely if referred to a standard or control model solution rather than to the analysis itself, due to the disparity between the resolution of the model and the analysis. For this reason, a control simulation is defined with the model characteristics given in Table 1 (the domain used is shown

TABLE 1. Summary of limited-area model parameters.

Horizontal grid:
E-grid (Arakawa notation)
Domain:
Low res. 105°W–45°W; 22°N–48°N
High res. 90°W–61.2°W; 26°N–42°N
Resolution:
horizontal—Low res. 1.0° lat. by 1.25° long.
High res. 0.32° lat. by 0.40° long.
vertical—9 sigma levels
Rainfall parameterization:
large-scale condensation and moist convective adjustment
Surface-layer fluxes:
Land—Proportional to surface height
Ocean—Proportional to lowest-level wind
Vertical diffusion in boundary layer:
Prandtl mixing length ("K") theory
Upper boundary condition:
Rigid lid at 1.98 mb
Radiation:
Fels-Schwarzkopf radiative transfer algorithms
Albedo:
Proportional to surface type and solar zenith angle
Soil moisture:
Balance of evaporation, precipitation, and snow melt
Lateral boundary conditions:
One-way inward feed only
Modified sponge and upstream advection in buffer region around border.

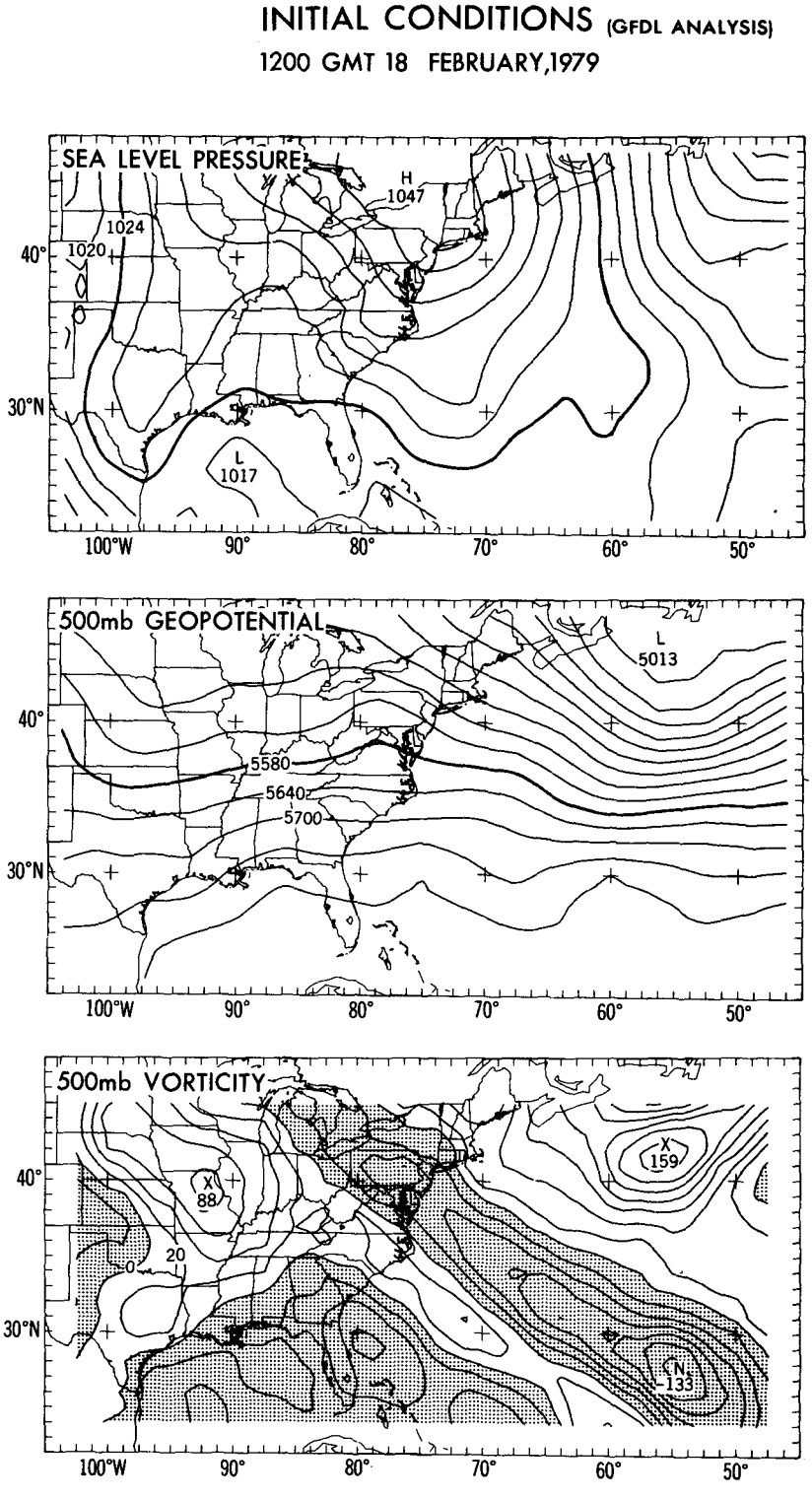

FIG. 4. Initial conditions for control simulation at 1200 UTC 18 February from GFDL analysis. Top panel is sea level pressure (contour interval = 4 mb with 1024 mb contour darkened). Middle panel is 500 mb geopotential (contour interval = 60 m with 5580 m contour darkened). Bottom panel is 500 mb relative vorticity (contour interval = 20×10^{-6} s^{-1} with negative values shaded).

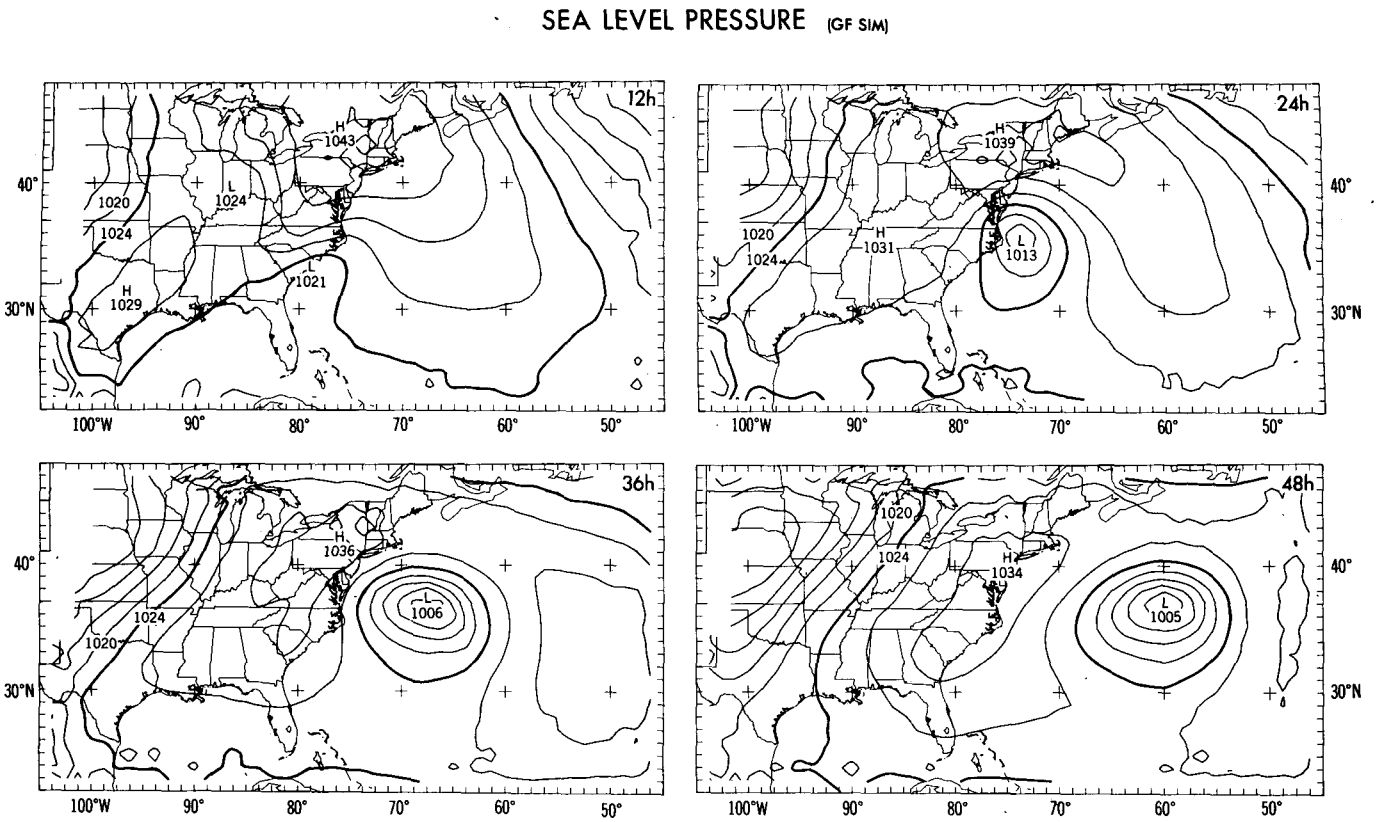

FIG. 5. Sea level pressure from control simulation for period 0000 UTC 19–1200 UTC 20 February 1979. Contour interval = 4 mb with 1024 mb contour darkened.

in Fig. 4), using the GFDL/FGGE archived analysis as initial conditions. Although the approximate 3° spacing of this global analysis is quite coarse to capture the mesoscale features indicated in previous studies (e.g., Bosart, 1981; Bosart and Lin, 1984), the continuous data insertion of the analysis scheme can provide the larger-scale forcing or components of these features. Comparisons between various model solutions and the control will be made to determine the sensitivity of the model to various factors. Root-mean-square (rms) differences of the 500 mb geopotential between the analysis and the model solutions are presented in section 8.

The time chosen to start the simulation and forecasts was 1200 UTC 18 February, in order to model the initial development of the low (around 0000 UTC 19 February) and the major deepening around 1200 UTC 19 February, while not having these features occur too long after the initial conditions. The initial GFDL/FGGE fields of sea level pressure, 500 mb heights and relative vorticity are shown in Fig. 4. The inverted trough in the Midwest at the surface associated with the short wave aloft is evident. Surface ridging is apparent along the East Coast. A large cyclonic storm is located at the northeast corner of the domain, as seen in both the 500 mb geopotential (middle graph of Fig. 4) and the relative vorticity fields (lower graph of Fig. 4). The maximum of relative vorticity over Missouri (88×10^{-6} s^{-1}) is associated with the short-wave trough. Large negative relative vorticities, apparent in the southeast corner of the domain, are similar to those noted in the analysis 12 hours later (see Fig. 3). The time-dependent boundary conditions for the control simulation were provided by the analyses shown in Figs. 1–3. The maps of the sea level pressure, 500 mb heights and 500 mb relative vorticity for every 12 hours of the control simulation to 48 hours are shown in Figs. 5–7, respectively. These can be compared to the GFDL/FGGE analyses in Figs. 1–3. An important factor to remember is that the grid used for the analysis had an equivalent spacing of 3° (~300 km), while the limited-area model grid spacing is 1.25° × 1.0° (approximately 1.6° or ~150 km between like grid points).[4] The global analysis is not the best analysis with which to compare the model since the model can produce more detailed features. However, comparison with the analysis that provided the initial and boundary conditions can quantify the general accuracy of the model simulation.

[4] Throughout the rest of this paper, the resolution of the model will be given as the number of equivalent degrees between like grid points on the E-grid (i.e., 1.6°).

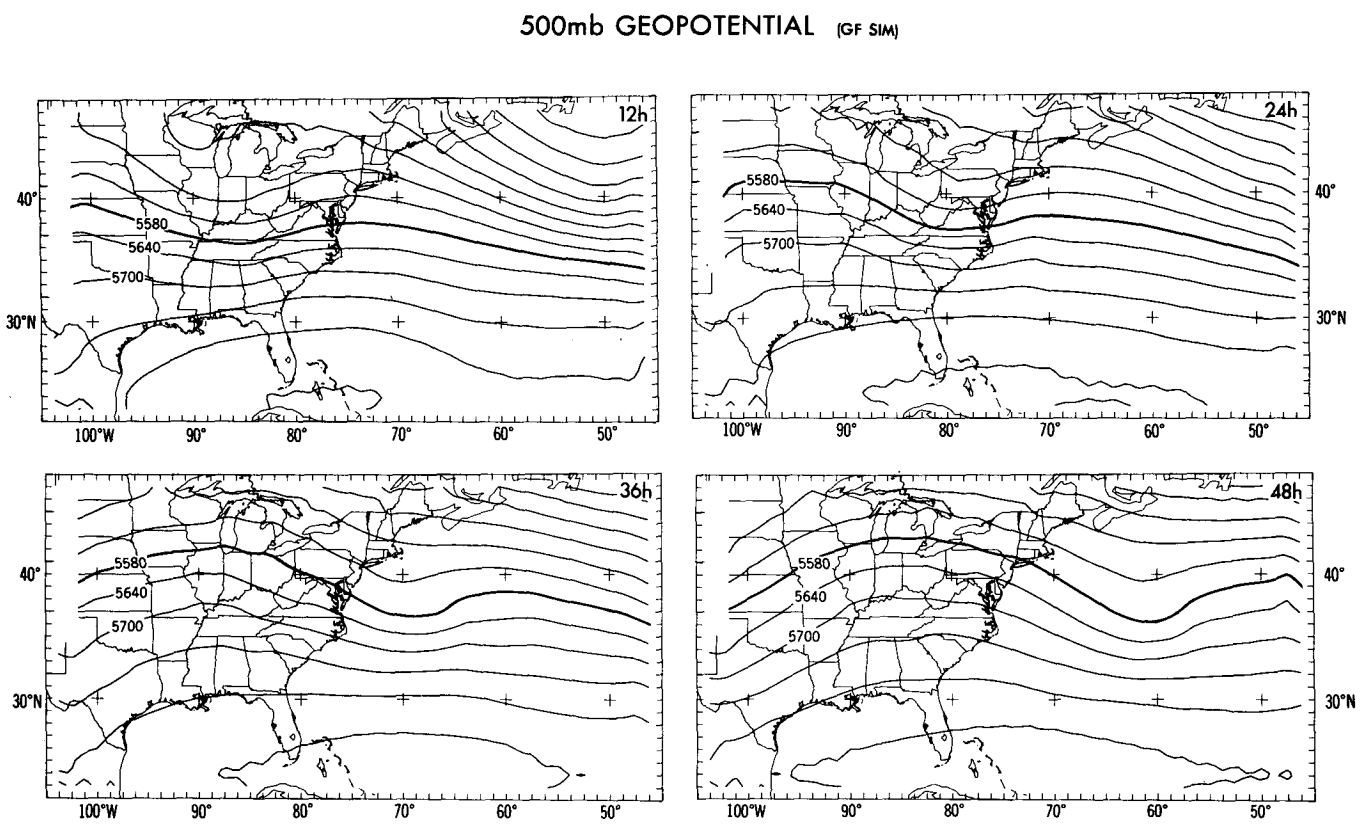

FIG. 6. 500 mb geopotential heights from control simulation for same times as Fig. 5. Contour interval = 60 m with 5580 m contour darkened.

In general, the sea level pressure of the simulation (Fig. 5) is similar to the analysis (Fig. 1). The low initially develops nearer to the coast, but at 24 hours (1200 UTC 19 February) and later, the positions and intensities are similar. The gradients in the simulation around the low are larger than in the analysis, associated with the finer resolution of the limited-area model. The simulation has a slightly more intense high over New England at 24 hours (1039 mb) and along the East Coast after 36 hours.

The 500 mb geopotential field of the simulation (Fig. 6) compares reasonably well with the corresponding analysis (Fig. 2) during the entire period modeled. However, the short wave in the numerical simulation is weaker than in the analysis during the first 24 hours. These discrepancies are less apparent after 24 hours. At this level, not much difference in the gradients is apparent.

The comparison of the 500 mb relative vorticity between the simulation (Fig. 7) and the analysis (Fig. 3) is similar to that of the 500 mb geopotential. The vorticity maximum of the Midwest short wave in the simulation decreased to 77×10^{-6} s^{-1} during the first 24 hours, while the analysis increased to 129×10^{-6} s^{-1}. At 36 hours, the vorticity maximum in the simulation has increased to 119×10^{-6} s^{-1}, similar to the analysis (122×10^{-6} s^{-1}). However, the analysis has a wave pattern south of the vorticity maximum not evident in the simulation. At 48 hours, the vorticity maximum of the short wave in the simulation appears to be more realistic with an organized center, while the analysis has considerable lack of coherence. An additional aspect to note is the ability of the model to treat the large negative relative vorticities in the initial conditions located in the southeast portion of the model domain by decreasing their magnitude and allowing them to propagate out of the domain.

In general, compared to the global analysis, the model captured the development and movement of the surface low reasonably well. Aloft, the model accurately simulated the movement of the short wave, while some discrepancy exists between the analysis and the model with regard to the intensity of the short wave during the first 24 hours. However, the short wave in the simulation was similar to the analysis after 24 hours.

Simulations initialized from the ECMWF, NMC, and GLAS analyses have been executed with the same model parameters that characterize the GFDL (control) simulation (see Table 1) and are discussed in the next section.

5. Impact of initialization

The ECMWF/FGGE, NMC, and the GLAS analyses have been used to provide initial and boundary conditions for the limited-area model primarily to test the

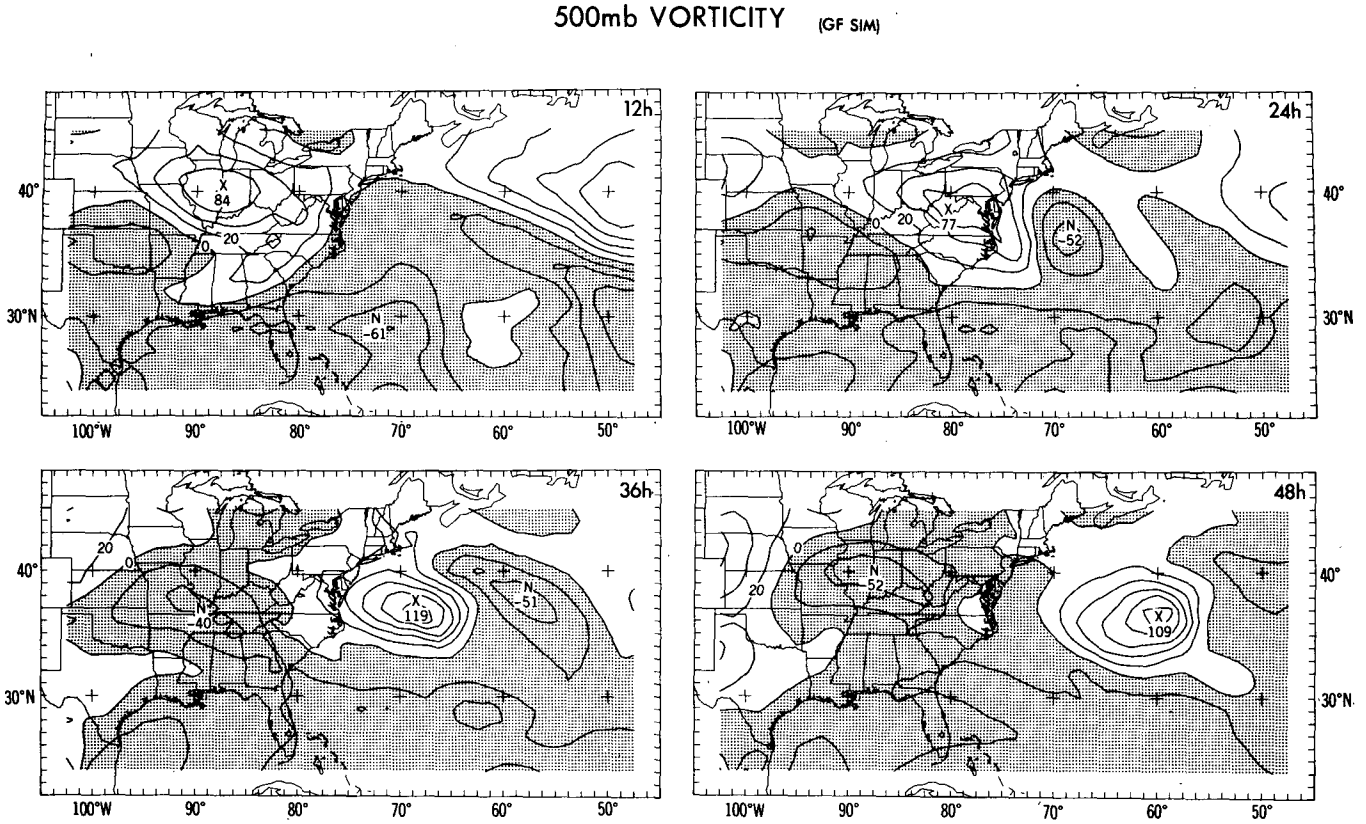

FIG. 7. Vertical component of 500 mb relative vorticity from control simulation for same times as Fig. 5. Contour interval = 20×10^{-6} s^{-1} with negative values shaded.

sensitivity of the model solution to the initial conditions. Ideally, for the study of the impact of the initial conditions on the quality of the forecast it is desirable to have random errors in the initial conditions. However, since all these analyses used different assimilation schemes and resolutions, comparisons between the simulations initialized with these various analyses can provide some measure of the impact of these features on the model solutions. The ECMWF/FGGE analysis is derived from a global four-dimensional analysis scheme (see Bengtsson et al., 1982) and has a horizontal resolution of 1.875°. A nonlinear normal mode initialization procedure has been used. The standard operational NMC global gridded analysis is used (see McPherson et al., 1979) with a horizontal resolution of 2.5°. The GLAS analysis is obtained from another four-dimensional analysis scheme (see Baker, 1983) and had a horizontal resolution of 4° × 5°. First, these three analyses are compared to the GFDL/FGGE analysis for the initial time (1200 UTC 18 February) in order to document their differences and similarities. The simulations using these alternative analyses are then compared to the control simulation at 24 hours. Finally, the track and intensity of the surface low and the 500 mb relative vorticity maximum are compared for the various analyses and simulations.

A comparison of the three different analyses with the GFDL analysis is shown for sea level pressure differences (Fig. 8) and 500 mb geopotential differences (Fig. 9). Negative differences imply lower pressures or heights for these additional analyses compared to the GFDL analysis.

In general, the sea level pressure analyses seem to be rather similar, with differences generally less than 2 mb. The differences of these analyses with the GFDL/FGGE analysis also seem to have some similarities. For instance, the positive anomalies along the western boundary of the domain are similar, perhaps due to the different mountain representations in the various analyses causing corresponding differences in the global model forecasts used as a first guess and in the treatment of the boundary layer. Also note that the analyses with the most coarse horizontal resolution (GLAS and GFDL) have the smallest differences in this region. The negative anomaly off the southeast coast of the U.S. is also quite similar in all the analyses, indicating a possible problem in the GFDL analysis. However, studies like Lau (1985) or Kung and Tanaka (1983) have shown that global statistics from the GFDL analysis are of comparable quality to the ECMWF analysis.

There is considerable similarity of the differences in the 500 mb geopotential between the various analyses and the GFDL analysis at 1200 UTC 18 February (Fig. 9). However, the differences are generally less than 60

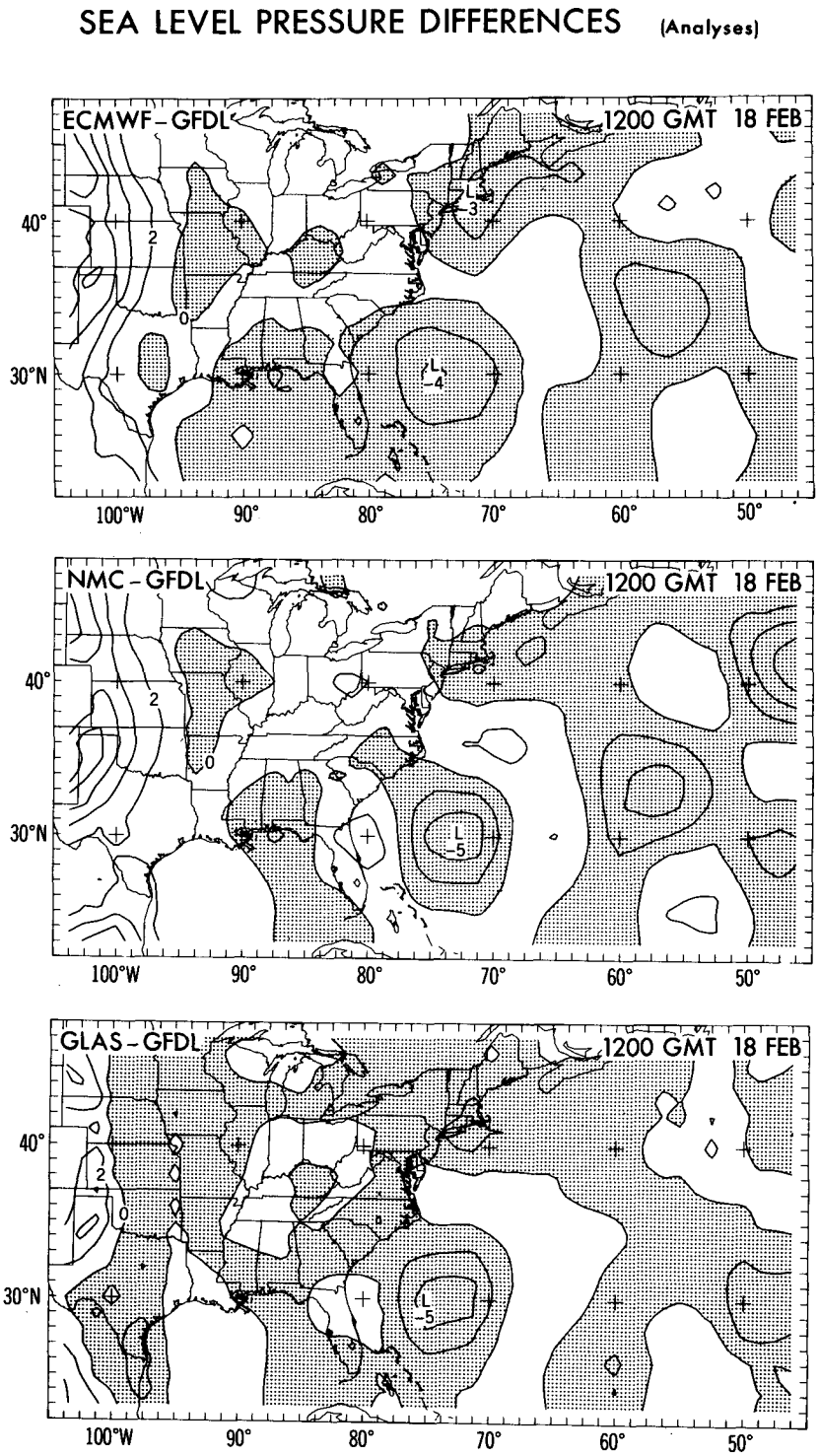

FIG. 8. Sea level pressure differences at 1200 UTC 18 February between ECMWF and GFDL analyses (top panel), NMC and GFDL analyses (middle panel), and GLAS and GFDL analyses (bottom panel). Contour interval = 2 mb with negative values shaded.

m, with the root-mean-square (rms) of the 500 mb geopotential field differences being 28 m for ECMWF-GFDL, 36 m for NMC-GFDL, and 40 m for GLAS-GFDL analyses. In both the ECMWF and the NMC analyses, the differences over the Rocky Mountains along the western boundary of the domain are similar to those described for the sea level pressure and are probably caused by similar reasons. Note that the rep-

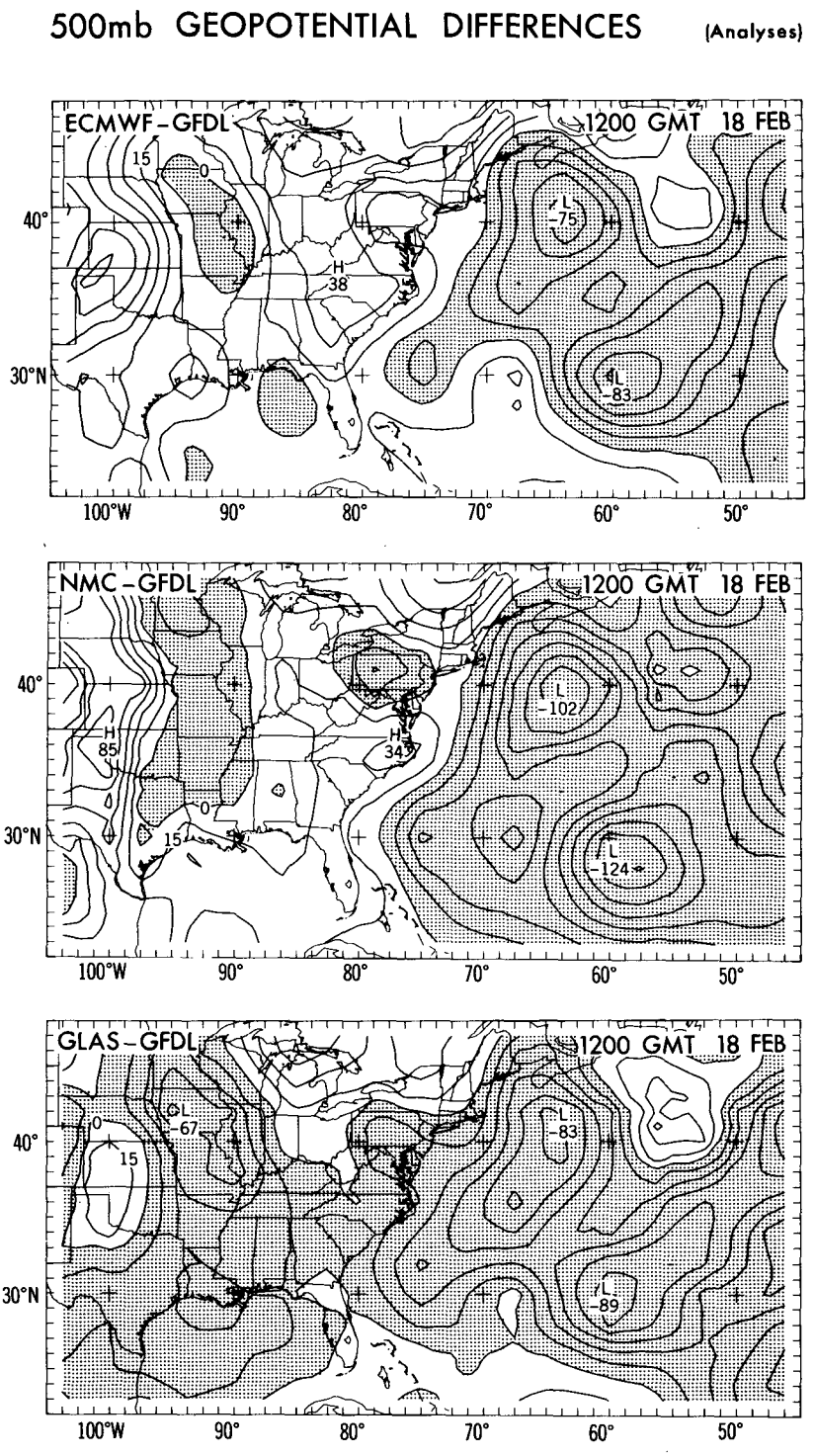

FIG. 9. 500 mb geopotential differences at 1200 UTC 18 February for same analyses and same format as Fig. 8. Contour interval = 15 m with negative values shaded.

resentation of the short-wave trough over Iowa is also different in the various analyses, with the ECMWF analysis having more intense ridges than GFDL both west and east of the trough axis, while the GLAS anal- has similar ridges but a deeper trough than GFDL. Over the ocean, the anomalies possibly result from the different first guesses used in the analyses in conjunction with the lack of observations.

The differences of sea level pressure and 500 mb heights at 1200 UTC 19 February in the three 24-h

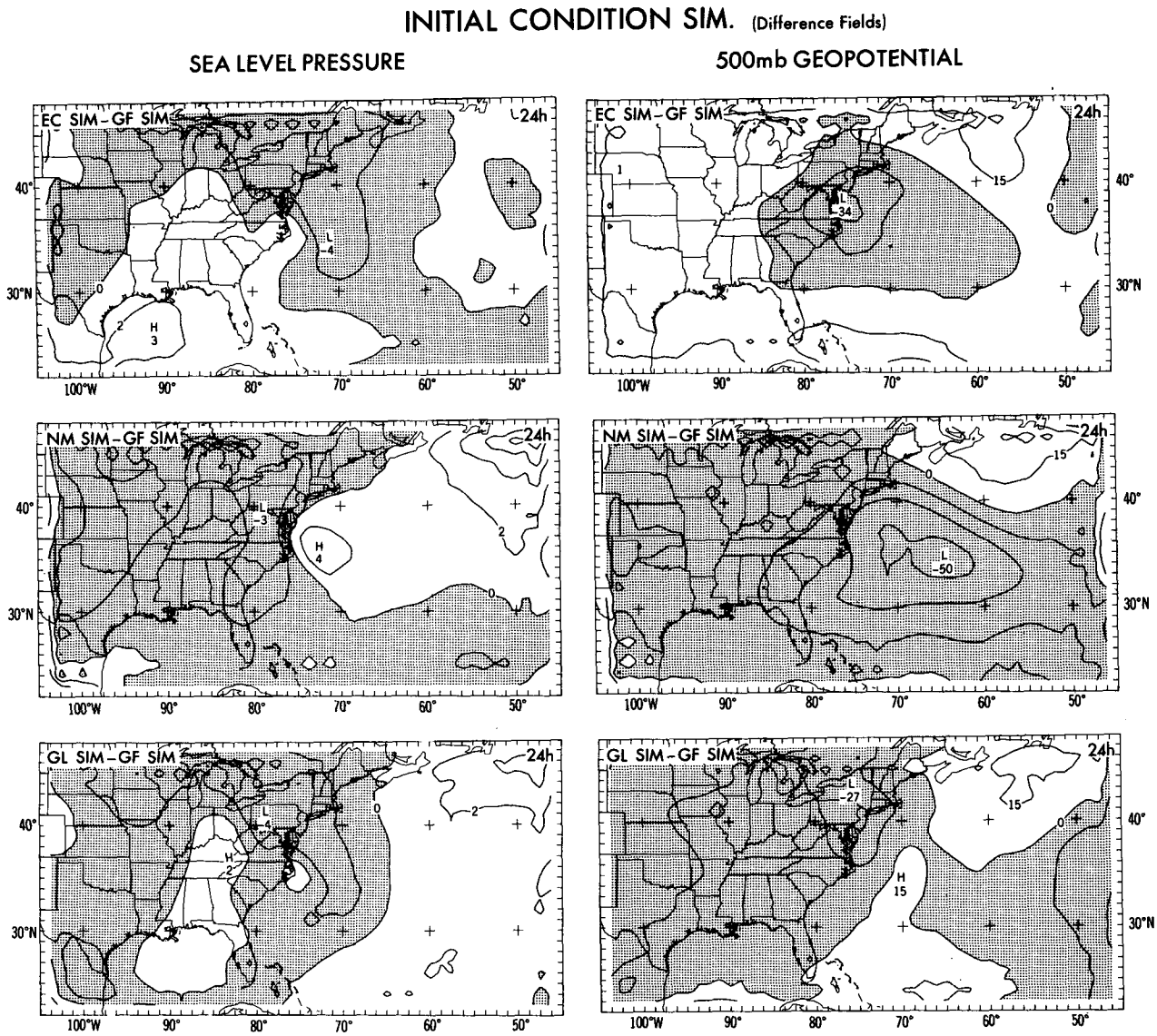

FIG. 10. Sea level pressure differences (left half, contour interval = 2 mb) and 500 mb geopotential differences (right half, contour interval = 15 m) of 24 h simulations: EC SIM − GF SIM (top row), NM SIM − GF SIM (middle row), and GL SIM − GF SIM (bottom row) (negative values shaded).

simulations using the different analyses as compared to the control simulation are shown in Fig. 10. Negative values occur when values in the new simulation are less than in the control simulation. Throughout the rest of this paper, the model runs are denoted by the first two letters of the analysis used for initial conditions; for example, EC SIM is the limited-area simulation initialized with the ECMWF analysis. A summary of the model experiments performed is shown in Table 2.

In general, all simulations were similar, with differences of sea level pressure and 500 mb height typically less than 4 mb and 30 m, respectively. Note that these differences are less than or equal to the differences in the initial conditions. Therefore, the differences in the initial conditions may not have been as significant for the model as they seemed. Evidently, the model adjusted some of the various inconsistencies between the analyses to a state that was more consistent with the model dynamics and thermodynamics. However, it is important to point out that the various simulations still have differences.

The EC SIM sea level pressure at 24 hours is over 2 mb deeper east and north of the low and less than 2 mb higher just west of the low. This results from the low in the EC SIM being slightly faster and deeper than in the control. The EC SIM 500 mb trough is just over 30 m deeper than the control over the low. This is

TABLE 2. Summary of sensitivity experiments (× means model run was executed).

Mode	Horizontal grid spacing	Parameter adjusted	Initial data analysis			
			GFDL	ECMWF	NMC	GLAS
Simulation	1.00° lat. 1.25° long.	Initial conditions	control ×	×	×	×
		Diffusion	×			
		Latent heat	×			
	0.32° lat. 0.40° long.	Horizontal resolution	×	×		
Forecast	1.00° lat. 1.25° long.	Lateral boundary conditions	×	×		

consistent with the more intense initial ECMWF short wave (Fig. 9) and the slightly deeper simulated low than in the control simulation.

The surface low at 24 hours in the NM SIM is less intense and located slightly west of the control simulation, resulting in higher pressures east and around the low, and lower pressures west of the low. At 500 mb, the generally lower heights evident ahead of the surface low are indicative of less ridging ahead of the short wave and is probably related to the weaker surface system.

The sea level pressure in the 24 hour GL SIM is over 2 mb deeper east and north of the control simulation low. The low in this simulation is northeast of the control simulation. Only minor differences can be seen at 500 mb between the GL SIM and the control simulation, with the short-wave trough only slightly deeper.

The tracks of the minimum sea level pressures for the various analyses and simulations are shown in Fig. 11. The analyses generally have similar tracks. The GFDL-analyzed low was southwest of the other analyses at 48 hours.

The minimum sea level pressure tracks of the various simulations are generally similar to the analyses. However, the surface lows are initially closer to the coast, especially for the GF SIM, in agreement with the storm track given by Bosart (1981). The NM SIM tended to be slower and south of the other simulations after 36 hours.

The temporal evolution of the minimum pressure of the analyses and simulations is shown in Fig. 12. The ECMWF analysis was generally deeper than the other analyses. The GLAS analysis developed a surface low slightly later than the GFDL and ECMWF analyses, but then deepened rapidly to become almost as deep as the ECMWF analysis at 48 hours. The GFDL and NMC analyses are similar except for the lack of a pressure minimum in the NMC analysis until 24 hours. These differences should not be surprising, considering the disparity in the model physics and resolutions for the various analyses. However, it seems rather surprising that both the highest-resolution ECMWF and lowest-resolution GLAS analyses are considerably deeper than the other analyses after 30 hours.

The simulated sea level pressure minima are fairly consistent with their corresponding analyses, although the simulated minimum sea level pressures are generally higher than the corresponding analyses, especially after 36 hours. The EC SIM develops the lowest pressure even though it was weaker than the GF SIM at 12 hours. The NM SIM was weaker than all the others, consistent with the corresponding analysis. Finally, the GL SIM, although initially weak, developed in intensity

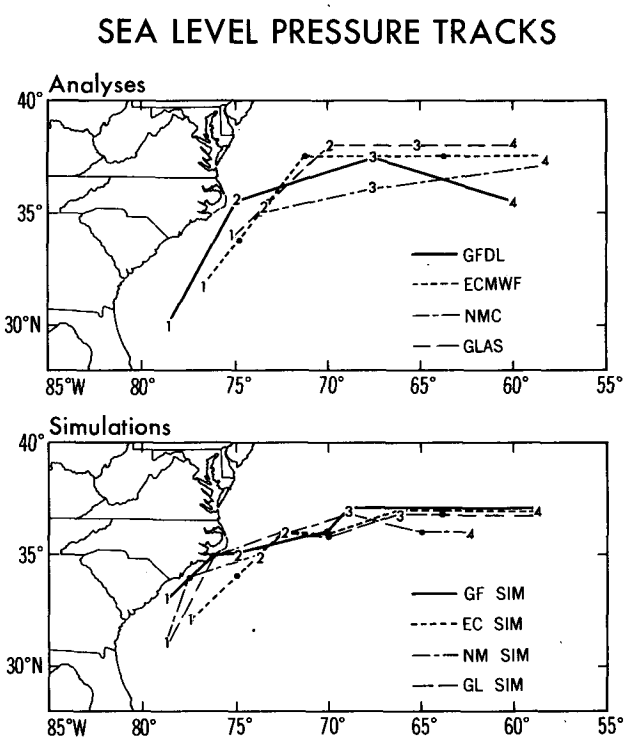

FIG. 11. Tracks of sea level pressure minimum in analyses (top panel) and simulations (bottom panel) (1: 0000 UTC 19 = 12 h; 2: 1200 UTC 19 = 24 h; 3: 0000 UTC 20 = 36 h; 4: 1200 UTC 20 = 48 h).

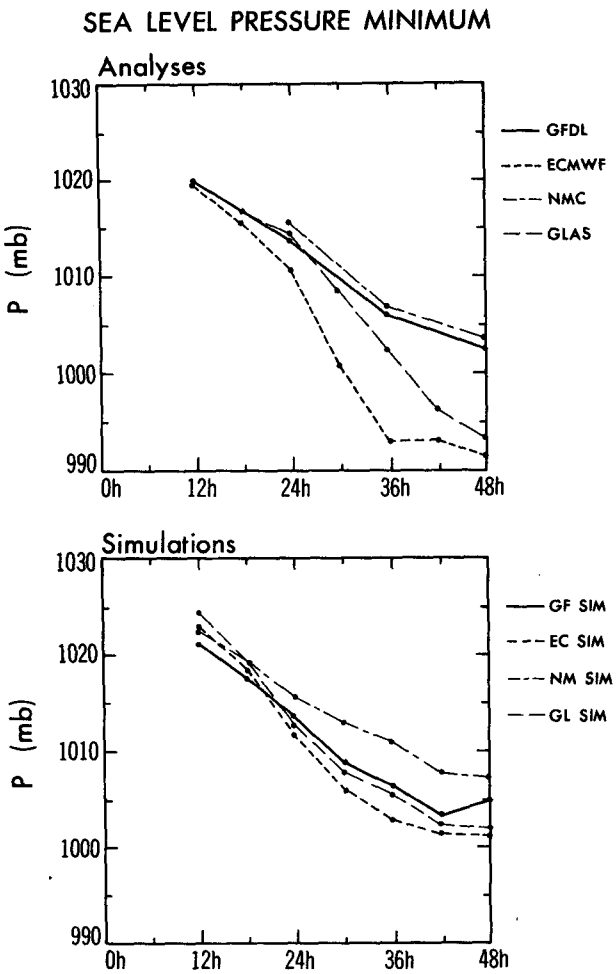

FIG. 12. Time evolution of sea level pressure minimum in analyses (top panel) and simulations (bottom panel).

to a value close to the EC SIM in a manner similar to the analyses. Notice that the evolution of the low in the four simulations has less variation between each other than between the four corresponding analyses. This can be partly attributed to the differences in resolution, first-guess fields used, and methods of assimilation between the analyses, while all simulations have the same resolution, dynamical and thermodynamical constraints and boundary layer treatment.

The magnitudes of the 500 mb relative vorticity maximum associated with the short wave propagating from the Midwest for the analyses and simulations are shown in Fig. 13. All tend to show a general increase in relative vorticity during the first 24 hours, followed by decreases to 48 hours. The ECMWF analysis shows a much stronger vorticity maximum than the other analyses, whereas the GLAS analysis has the weakest vorticity maximum after the initial time. This is consistent with the resolution differences of the analyses.

A marked difference can be seen between the simulated and the analyzed 500 mb relative vorticity. All simulations show a nearly constant or a slight decrease in the relative vorticity maximum until 24 hours, followed by an increase to 30–36 hours, with a fairly constant vorticity until 48 hours. The explanation of the discrepancy of the intensity of the short wave between the analyses and the simulations is not clear and is presently under investigation.

The short wave apparently had little effect on the *initial* development of the low since all simulations did a reasonable job in simulating the development of the surface low. The predicted locations of the low during the first 18 hours were well simulated. After 18 hours, when the short-wave trough reached the coast and interacted with the surface low, the lack of intensity of the short wave in the simulations may have precluded prediction of the stronger deepening of the surface low between 24 and 36 hours in the analyses.

6. Impact of horizontal diffusion and latent heat

The lack of development for the first 24 hours in the simulations' 500 mb relative vorticity possibly may be

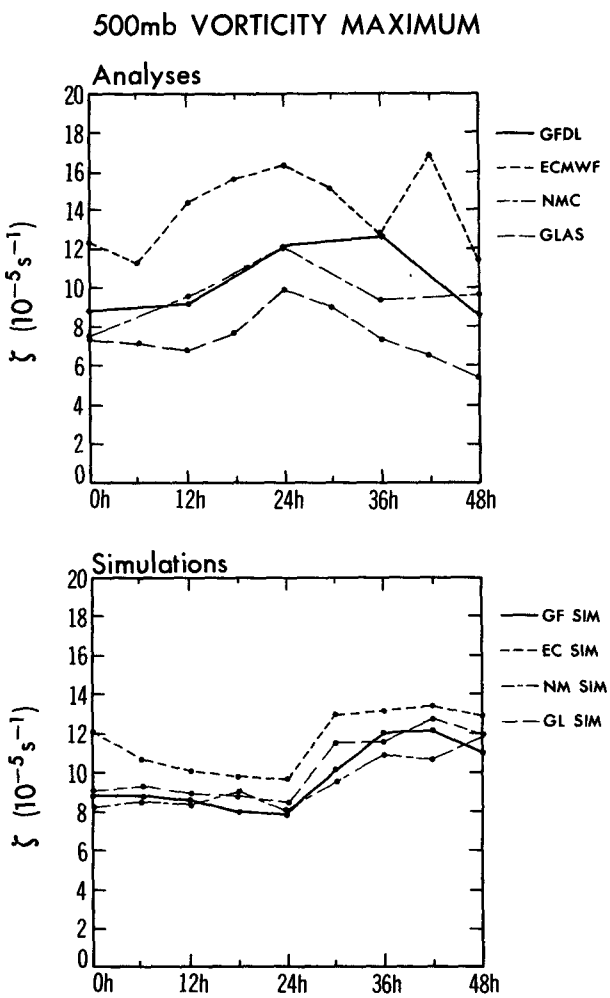

FIG. 13. Time evolution of the vertical component of 500 mb relative vorticity maximum for shortwave in analyses (top panel) and simulations (bottom panel).

attributed to the horizontal diffusion used being too large. Another possible cause for the lack of early vertical development can be attributed to the effect of the latent heat release in developing the surface cyclone vertically. A few experiments have been performed in order to elucidate the sensitivity of the simulation to these parameters.

As expected, the system became more intense (lower sea level pressure and larger 500 mb relative vorticities) with lower horizontal diffusion (Fig. 14). The behavior of the 500 mb vorticity maximum was generally the same, with nearly constant magnitude for the first 24 hours followed by increases associated with the coastal cyclone except for the low (1×10^5 m^2 s^{-1}) and high (5×10^6 m^2 s^{-1}) diffusion cases. Although the low-diffusion case appears to have captured the development of the upper trough, the solution exhibits an unacceptable level of noise from 24 hours onward. In the high-diffusion case, the surface low was so severely damped that it did not develop vertically. The differences in the development due to changes in the diffusion were larger than the differences associated with the various initial conditions.

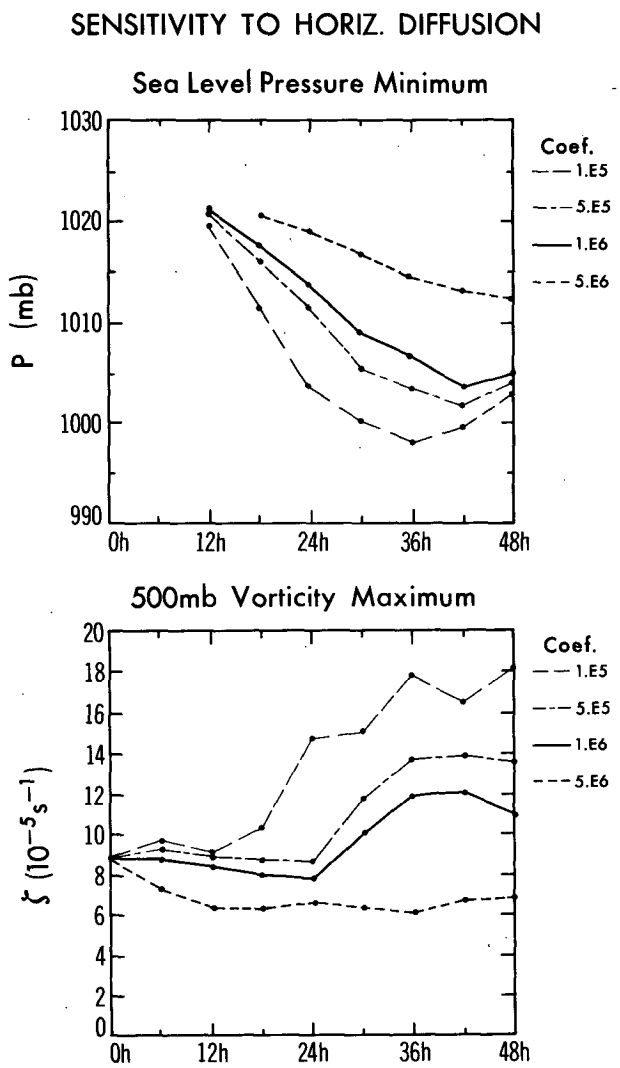

FIG. 14. Time evolution of sea level pressure minimum (top panel) and 500 mb relative vorticity maximum (bottom panel) for the GF simulations with varying horizontal diffusion coefficients (units m^2 s^{-1}; control simulation diffusion = 1.0×10^6).

The importance of latent heat release for the development of this storm has been mentioned by Atlas (1987), Bosart (1981) and Uccellini et al. (1983). This was tested in this study by preventing all latent heat release in the control simulation. The differences of sea level pressure and 500 mb heights at 24 hours between the no-latent heat and control simulations are presented in Fig. 15. Although a low did develop by 24 hours, it was much weaker and west of the control simulation. After 24 hours, it did not develop further and moved slowly northeastward (not shown). At 500 mb, the lack of latent heat resulted in less ridging ahead of the short wave and lacked the vorticity increases between 24 and 36 hours in the control simulation. Thus, latent heat was very important for the development of the surface low, and strongly influenced the upper-level flow. This is in accordance with the results of Atlas (1987). The effect of latent heating may also partially explain the discrepancy between the analysis and the simulations for the intensity of the short wave. The control simulation was deficient in precipitation amounts over land, and especially over Maryland (not shown). The lack of latent heating associated with this deficient precipitation may be related to the lack of development of the short wave.

7. Impact of horizontal resolution

The horizontal resolution of the control simulation was almost two times finer than the initial and boundary condition analyses. However, Orlanski et al. (1985) state that to adequately simulate the evolution of atmospheric fronts, the grid resolution should be no more than 50 km. The increase in accuracy of forecasting mesoscale features with a higher horizontal-resolution model was also mentioned by Kocin et al. (1985). Therefore, in order to more accurately simulate the development of the coastal cyclone, the horizontal grid resolution was decreased from 1.6° (~150 km) of the control to 0.5° (~50 km) in the high-resolution simulation. The domain size was also decreased from 26° latitude by 60° longitude for the control to 16° latitude by 28.8° longitude for the high-resolution simulation to limit the computational demands (domain used is shown in Fig. 16). The global GFDL and ECMWF analyses were used to provide the initial and boundary conditions for the high-resolution simulations.

The surface low in the high-resolution GF SIM is much more intense and is located north of the control simulation at this time (see upper frame of Fig. 16). At 500 mb, the geopotential trough is more intense (middle frame of Fig. 16) and the 500 mb relative vorticity maximum (not shown) is considerably larger (300

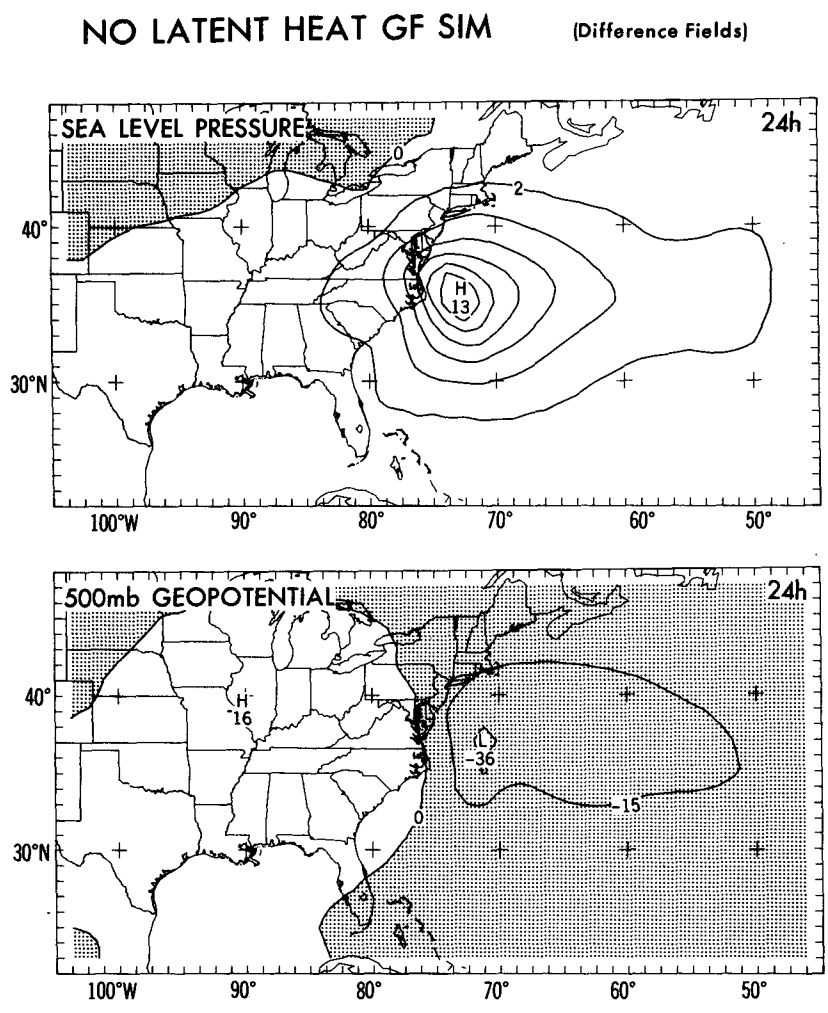

FIG. 15. Sea level pressure differences (top panel, contour interval = 2 mb) and 500 mb geopotential differences (bottom panel, contour interval = 15 m) at 24 h between GF SIM without latent heating and the control simulation (negative values shaded).

$\times 10^{-6}$ s^{-1}). As a result of more intense development, greater precipitation amounts occur in the high-resolution simulation (lower frame of Fig. 16).

In order to demonstrate the accuracy of the two high-resolution simulations, they are compared with the detailed mesoanalysis by Bosart (1981) (Fig. 17). A high degree of correspondence is evident. At 0600 UTC 19 February, the simulated low is northwest of the mesoanalysis, while at 1200 UTC 19 February, the low in the simulation is slightly south of the analysis, possibly indicating a slightly slower-moving system. The winds in the lowest sigma layer of the model generally agree very well with the observed surface winds, although the winds over land are more intense in the simulation, and the paucity of oceanic observations precludes a definitive statement. The surface air temperatures are fairly accurately simulated, although somewhat warmer along the coast and over the ocean. The coastal front has been well simulated, as determined by comparing the temperature gradients of the mesoanalysis and the simulation. For comparison, the fields are stated to be at sea level. However, the model winds and temperature are actually from the first sigma level above the surface (~75 m). In fact, if there is a very stable boundary layer over the cold land surface, the true model surface winds might be weaker and more in agreement with the analysis. In general, the simulation of precipitation is fairly successful near the low and moderate to poor northwest of the low. In particular, the 6-h precipitation area greater than 1 cm northwest of the low in the analysis is lacking in the high-resolution simulation. The cause of this deficiency is still under investigation. The model precipitation over the ocean cannot be verified due to lack of observations.

One problem with most mesoscale simulations is the lack of detailed analyses with which to verify the model solutions. Both the lack of temporal and spatial resolution in the standard upper-air network prevents detailed comparisons with observations. In this case in

HIGH HORIZ. RESOLUTION GF SIM (Difference Fields)

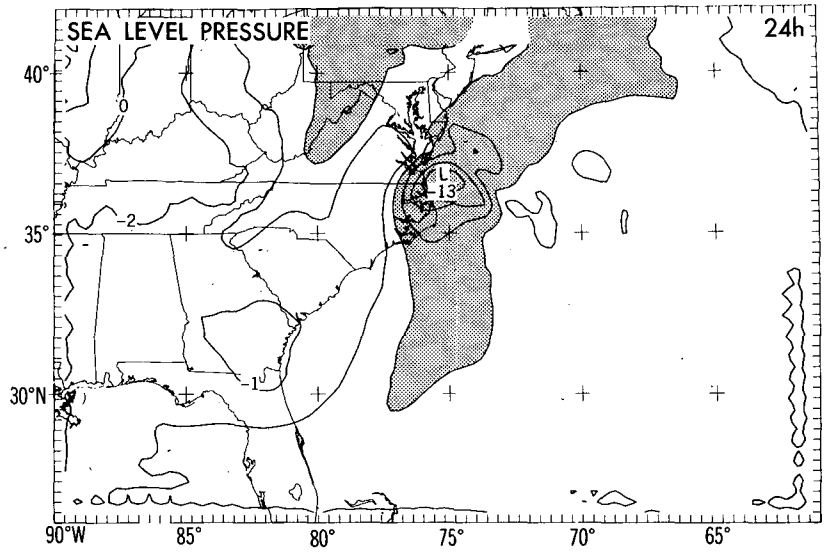

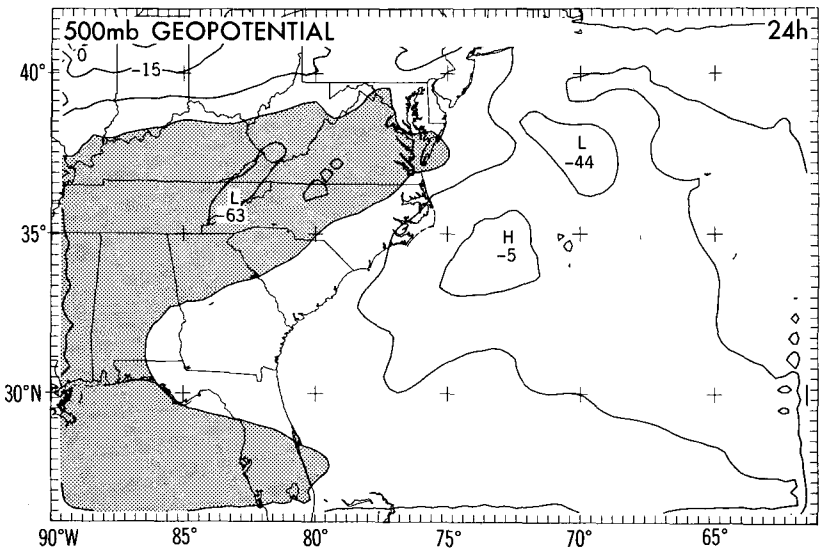

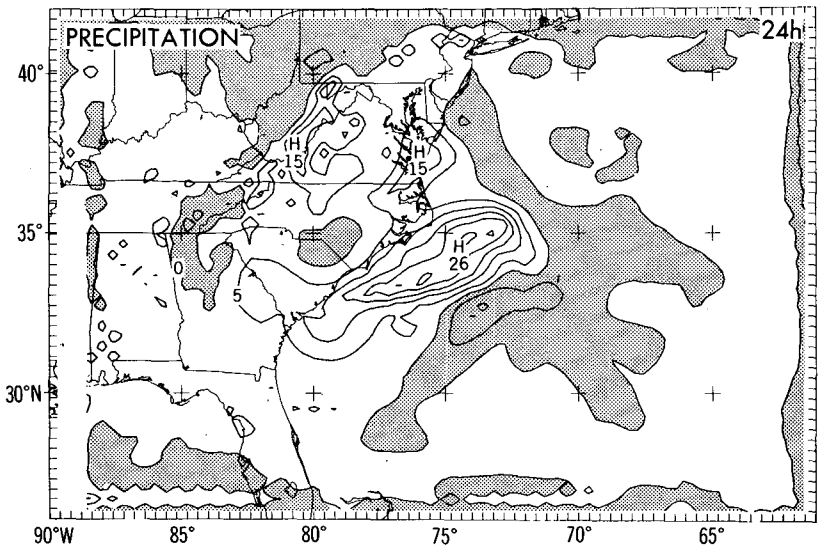

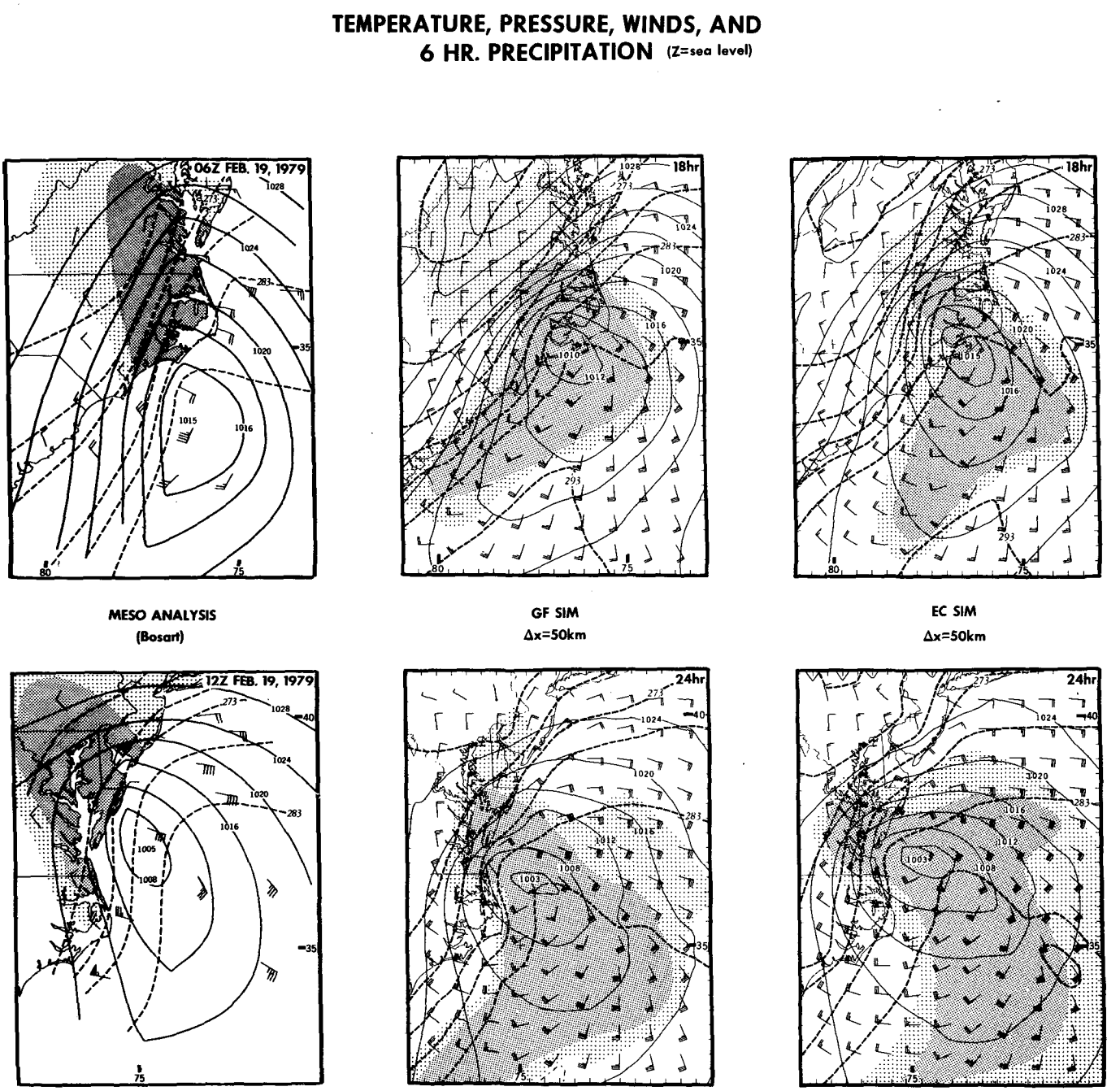

FIG. 17. Horizontal distributions of 18 and 24 h simulations on high horizontal resolution GF SIM (middle) and EC SIM (right) together with the corresponding observed distributions as analyzed from ship reports and local stations (left) (from Bosart, 1981). Winds (half barb = 2.5 m s^{-1}; full barb = 5 m s^{-1}), temperature (K, dashed), surface pressure (mb, solid), and 6-h accumulated precipitation (heavy shaded > 1 cm, light shaded between 0.5 cm and 1 cm). No precipitation observations are available over oceanic areas.

FIG. 16. High horizontal resolution GF SIM minus the control simulation at 24 h. Top panel: sea level pressure differences, contour interval = 2 mb, values less than −6 mb shaded. Middle panel: 500 mb geopotential height differences, contour interval = 15 m, value less than −45 m shaded. Bottom panel: Precipitation, contour interval = 5 mm, negative values shaded.

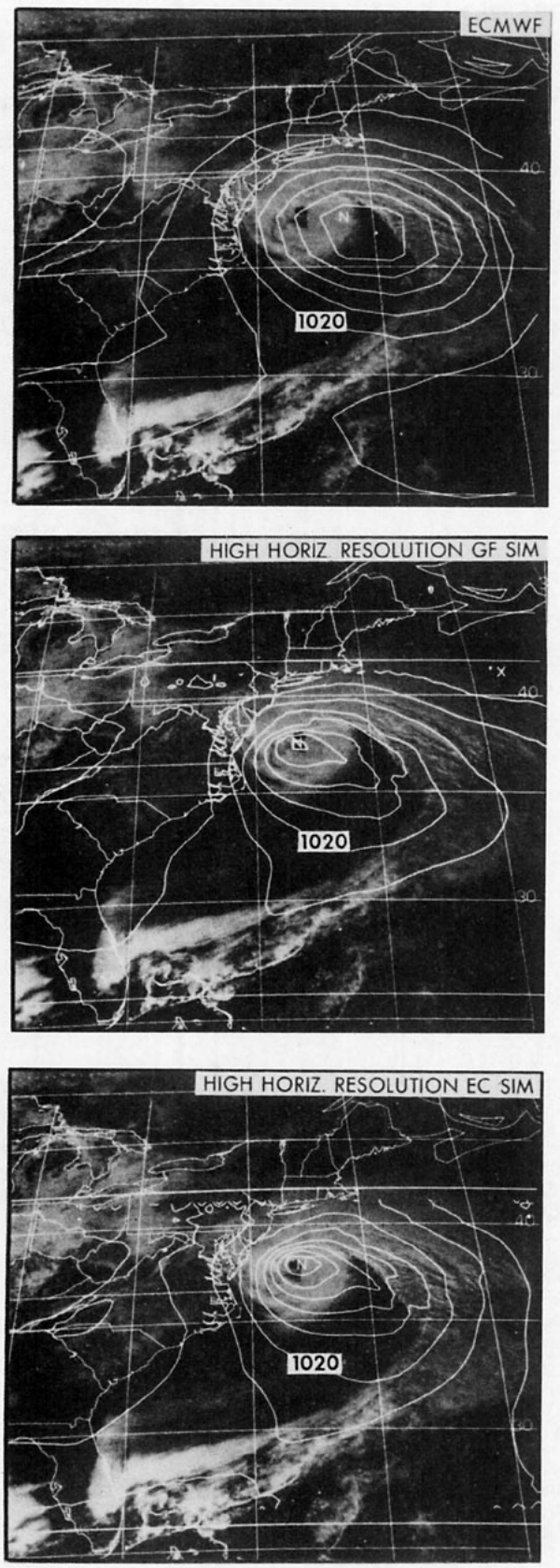

particular, the storm developed over the ocean with the resulting lack of observations. One method to help verify mesoscale models is to compare the model solutions to satellite imagery which has fairly high spatial and temporal resolution. Although the detailed upper-air structure cannot be determined using satellites, sometimes unique mesoscale features are apparent which can then be compared to the model solution. A comparison of the 1830 UTC 19 February visible satellite image with the 1800 UTC ECMWF analysis and the two high-resolution simulations (GF SIM and EC SIM) at 30 hours are shown in Figs. 18a and 18b for sea level pressure and surface relative vorticity, respectively. The ECMWF analysis is included here to document the general accuracy of the global analyses used for initial and boundary conditions and to demonstrate the improvement in accuracy of the simulations.

The sea level pressure comparison (Fig. 18a) shows that the analysis and the model solutions are close to the actual low position as indicated by the "eye" in the clouds. However, one can immediately see the lack of detail in the global analysis. First, the position is east of the actual low center. In addition, the lack of any cold frontal trough is apparent. This is not unexpected since the resolution of the analysis is only about 1.875°. In the two high-resolution simulations, some indication of a cold frontal trough is evident extending along the western edge of the clouds. In addition, the location of the surface low is much more accurate. Also note that both high resolutions are remarkably similar, especially considering the differences noted earlier in the analyses.

To further demonstrate the accuracy of the high-resolution simulation, a comparison of the 1830 UTC 19 February satellite picture with the surface relative vorticity for the ECMWF analysis and the high-resolution simulations (GF SIM and the EC SIM) at 1800 UTC (30 hours) is shown in Fig. 18b. The circulation center in the ECMWF analysis is generally near the storm center when viewed from the global perspective. However, the position of the center of the surface circulation in the analysis is about 200 km east of the center, as indicated by the satellite picture. This agreement is about as good as one can expect from this coarse analysis. The high-resolution simulations made significant improvements in both position and location compared to the global analysis, as one would expect. The vorticity maximum in both these simulations is located at the same position as the center of the circulation as indicated by the cloud distribution (the "eye").

FIG. 18a. Visible satellite cloud picture at 1830 UTC 19 February with sea level pressure data (contour interval = 4 mb) at 1800 UTC 19 February overlayed in same projection. Top panel: ECMWF analysis. Middle panel: High horizontal resolution GF SIM. Bottom panel: High horizontal resolution EC SIM.

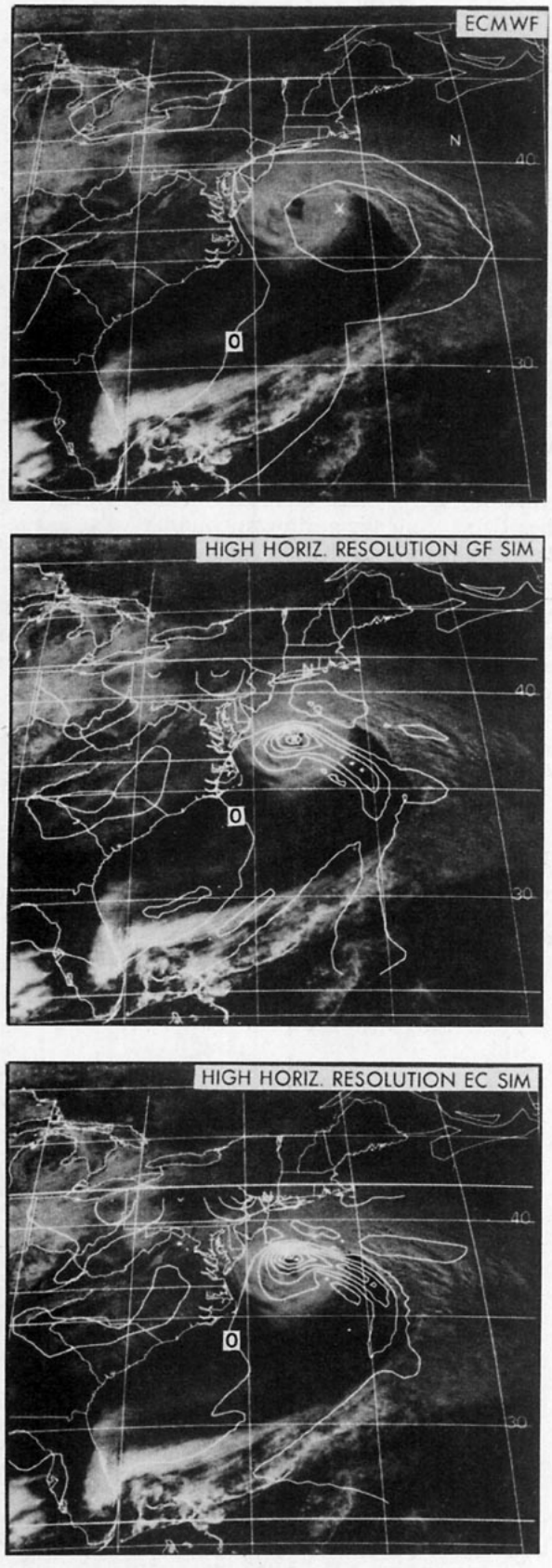

The axis of larger vorticities extending southeast and then southwest along the cold front in the simulations closely follows the cloud band. The model solutions are possibly slightly slower than observed, since this feature is slightly west of the cloud band. The high-resolution EC SIM is even closer in its positioning of the cold front, as indicated by the trough of lower pressure extending from the low and the axis of higher vorticity. An additional factor to consider in the placement of the cold front in the simulations is the 30-min time difference between the model solutions and the cloud distributions. As this was a fast-moving system, the cold front in the simulation would probably be slightly farther east 30 minutes later.

The most improvement in the sensitivity studies occurred through the increase in the horizontal resolution. The intensity of the surface vorticity along with the positioning and deepening of the low have benefited by more detail in the horizontal resolution. An additional side benefit, a result of the smaller computational domain, is the stronger influence of the analyzed data at the side boundaries, leading to a better description of the planetary environment in which the coastal cyclone develops. This effect will be more clearly seen in the next series of experiments where the lateral boundary conditions for the limited-area model come from the global spectral forecast rather than the analyzed fields.

8. Nested forecast

The results of the previous sections have the influence of the analyzed data through the lateral boundary for the entire period of integration. This is an optimal constraint because it is like "perfect" data. Unfortunately, in a numerical forecast mode, "perfect" data at the boundaries is not known. Data in this case should be provided by another forecast with a coarser-model resolution. The nested system used in this study consists of a global spectral model which provides boundary data to the limited-area model. To understand the uncertainties in the limited-area forecast that are produced by the imperfect boundary data, the global spectral forecast that provides data to the limited area model is discussed first.

a. Global spectral forecast

The global spectral model forecast used in the nested system will be discussed in this section. A summary of the global spectral model is given in Table 3 and in the

FIG. 18b. Visible satellite cloud picture at 1830 UTC 19 February with surface relative vorticity data (contour interval = 1×10^{-4} s^{-1}) at 1800 UTC 19 February overlayed in same projection. Top panel: ECMWF analysis. Middle panel: High horizontal resolution GF SIM. Bottom panel: High horizontal resolution EC SIM.

TABLE 3. Summary of global spectral model parameters.

Domain:
global
Resolution:
horizontal—R30 (transform grid = 2.25° lat. by 3.75° long.)
vertical—nine sigma levels
Rainfall parameterization:
large-scale condensation and moist convective adjustment
Surface-layer fluxes:
Bulk aerodynamic drag laws
Vertical diffusion in boundary layer:
Prandtl mixing length ("K") theory
Upper-boundary condition:
Rigid lid at 0 mb
Radiation:
Manabe-Strickler radiative transfer algorithms
Albedo:
Proportional to surface type and solar zenith angle
Soil moisture:
Balance of evaporation, precipitation, and snow melt
Lateral boundary conditions:
One-way outward feed only
Solutions every timestep interpolated to limited-area perimeter.

Appendix. The global spectral model forecast will be discussed first for the two initial fields: GFDL and ECMWF. As was done for the limited-area model, the spectral forecast will be denoted by the first two letters of the analysis used for initial conditions; for example, GF SPC is the spectral forecast initialized with the GFDL analysis. One should note that the GFDL archived analysis does not contain the nonlinear normal-mode initialization procedure. However, the global spectral model was started using the GFDL analysis after nonlinear normal-mode initialization.

The differences of the 500 mb heights between the GF SPC forecast and the GFDL analysis at 24 and 48 hours are shown in the top half of Fig. 19. At 24 hours, the spectral forecast has stronger ridging over the Mississippi Valley than the analysis does. The short-wave trough approaching the East Coast is not as deep in the spectral forecast as in the analysis. Elsewhere, the forecast and the analysis are similar. By 48 hours, the short-wave trough in the forecast was west of the analyzed trough and somewhat deeper. The trough approaching the western boundary of the domain and the ridging along the northwest boundary were less intense in the forecast than the analysis.

The differences of the 500 mb heights for the EC SPC forecast and its corresponding analysis at 24 and 48 hours are shown in the lower half of Fig. 19. In general, the 24-hour differences are slightly smaller than for the GF SPC forecast. The rms of the EC SPC fore-

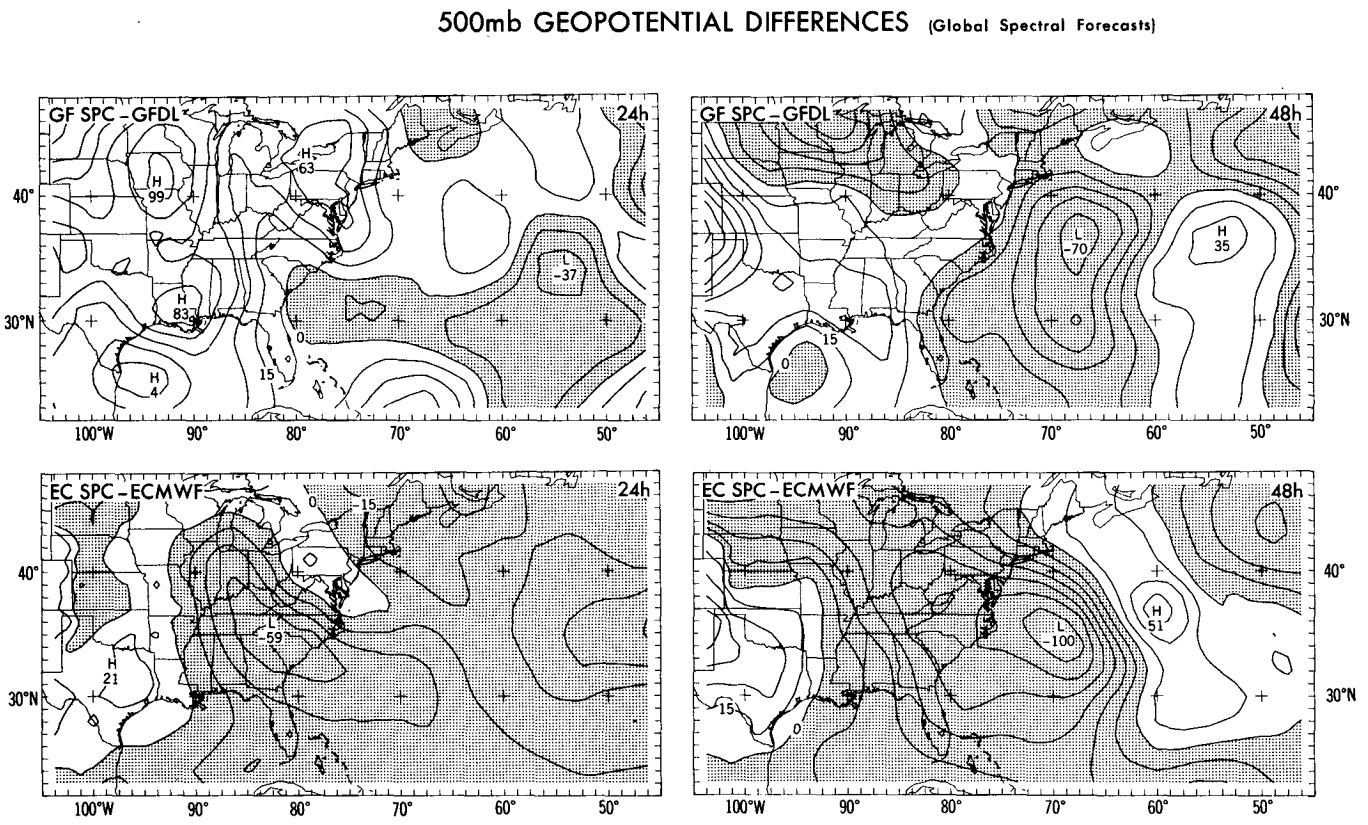

FIG. 19. 500 mb geopotential height differences at 24 h (left panel) and 48 h (right panel) between GF SPC forecast and GFDL analysis (top row) and between EC SPC forecast and ECMWF analysis (bottom row). Contour interval = 15 m with negative values shaded.

cast 500 mb heights over the low-resolution limited-area domain is about 25 m, while the GF SPC forecast had a rms of 38 m (both compared to their corresponding analysis). The forecasted 500 mb heights are lower than the analysis over most of the domain shown. The largest difference occurs over the Ohio Valley west of the propagating short wave, indicating slower movement and less ridging west of the wave.

At 48 hours, the 500 mb height differences of the EC SPC forecast are larger than for the GF SPC forecast. The rms for the EC SPC forecast (43 m) is significantly larger than for the GF SPC forecast, which stayed about the same. The differences are indicative of slower movement for the short wave in the EC SPC forecast than in the ECMWF analysis. Differences along the western boundary are similar to the GF SPC forecast.

The minimum sea level pressure and 500 mb relative vorticity maximum for the two spectral forecasts are shown in Fig. 20. The GF SPC forecast sea level pressure minimum is similar to the GFDL analysis (see Fig. 12). After 30 hours, the forecasted pressure minimum is lower than the analysis. The EC SPC forecast sea level pressure minimum is deeper than the ECMWF analysis through 24 hours and then becomes weaker. The spectral forecasts tend to be more similar to each other after 36 hours than to their respective analyses.

The maximum of 500 mb relative vorticity in the spectral forecasts (bottom of Fig. 20) shows a slow increase to 30 hours for both the GF SPC and the EC SPC cases. The GF SPC forecast shows considerable agreement with the GFDL analysis (Fig. 13), while the EC SPC forecast was more similar to the GF SPC forecast than the ECMWF analysis. This probably results from the use of the GFDL spectral model for the global forecasts which is similar to that used in the GFDL assimilation system and different from the ECMWF assimilation system. The considerable discrepancy of the initial relative vorticity between the ECMWF analysis and the spectral initial conditions from the same dataset is due to the relatively coarse spectral representation of the data.

Figure 21 shows the 1200 UTC 19 February ECMWF analysis and the 24-hour EC SPC forecast, EC SIM, and the high-resolution EC SIM of sea level pressure and surface winds and temperatures. The figure illustrates the differences in the minimum pressure obtained from the various model solutions: 1010 mb for the spectral model, 1012 mb for the EC SIM, and 1003 mb for the high-resolution EC SIM. Note, however, that the global analysis shows a minimum of 1011 mb, 6 mb higher than the observed minimum of 1005 mb (see Fig. 17). Clearly, the lack of detailed representation by the coarse initial data did not prevent the high-resolution simulation from accurately predicting the mesoscale structure of the low-pressure system (see discussion of Fig. 17). Moreover, these results indicate that high model resolution is required to produce accurate forecasts of the storm's structure, intensity, and position.

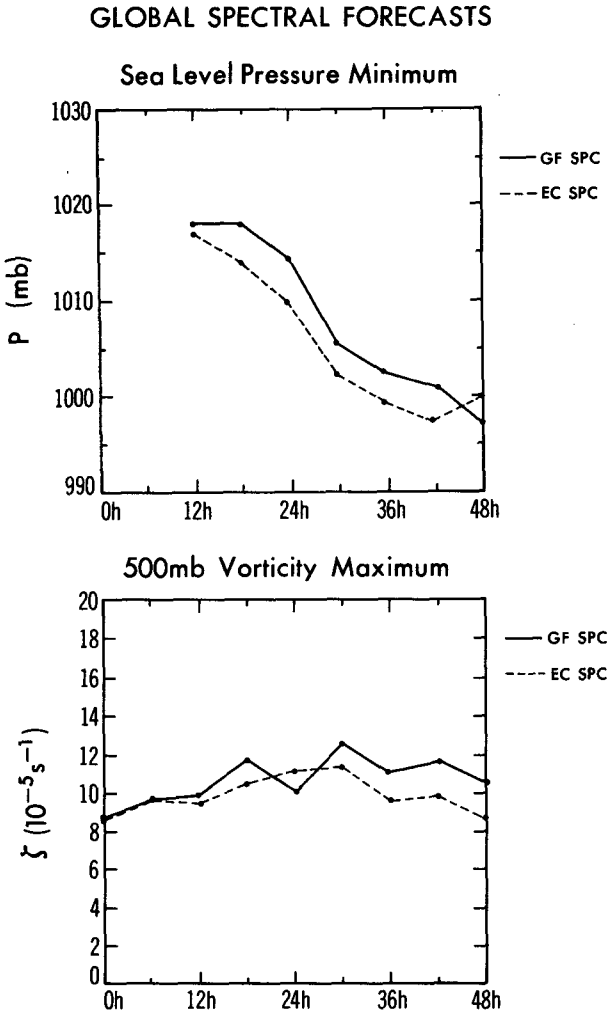

FIG. 20. Time evolution of sea level pressure minimum (top panel) and 500 mb relative vorticity maximum (bottom panel) for global spectral forecasts (GF SPC and EC SPC).

b. *Limited-area forecasts*

Two limited-area forecasts were executed: one with the GFDL analysis as initial conditions and the GF SPC providing boundary conditions (called GF FOR), and the other with the ECMWF analysis as initial conditions and using the EC SPC as boundary conditions (called EC FOR). The results are compared to the control simulation in this section. In this discussion, the initial conditions for the limited-area GF FOR were derived from the GFDL archived analysis that did not include the nonlinear normal-mode initialization.

The differences between GF FOR and GF SIM (control) of sea level pressure, 500 mb heights, and 500 mb relative vorticities are shown in Fig. 22. At 24 hours, the forecasted sea level pressure was generally similar

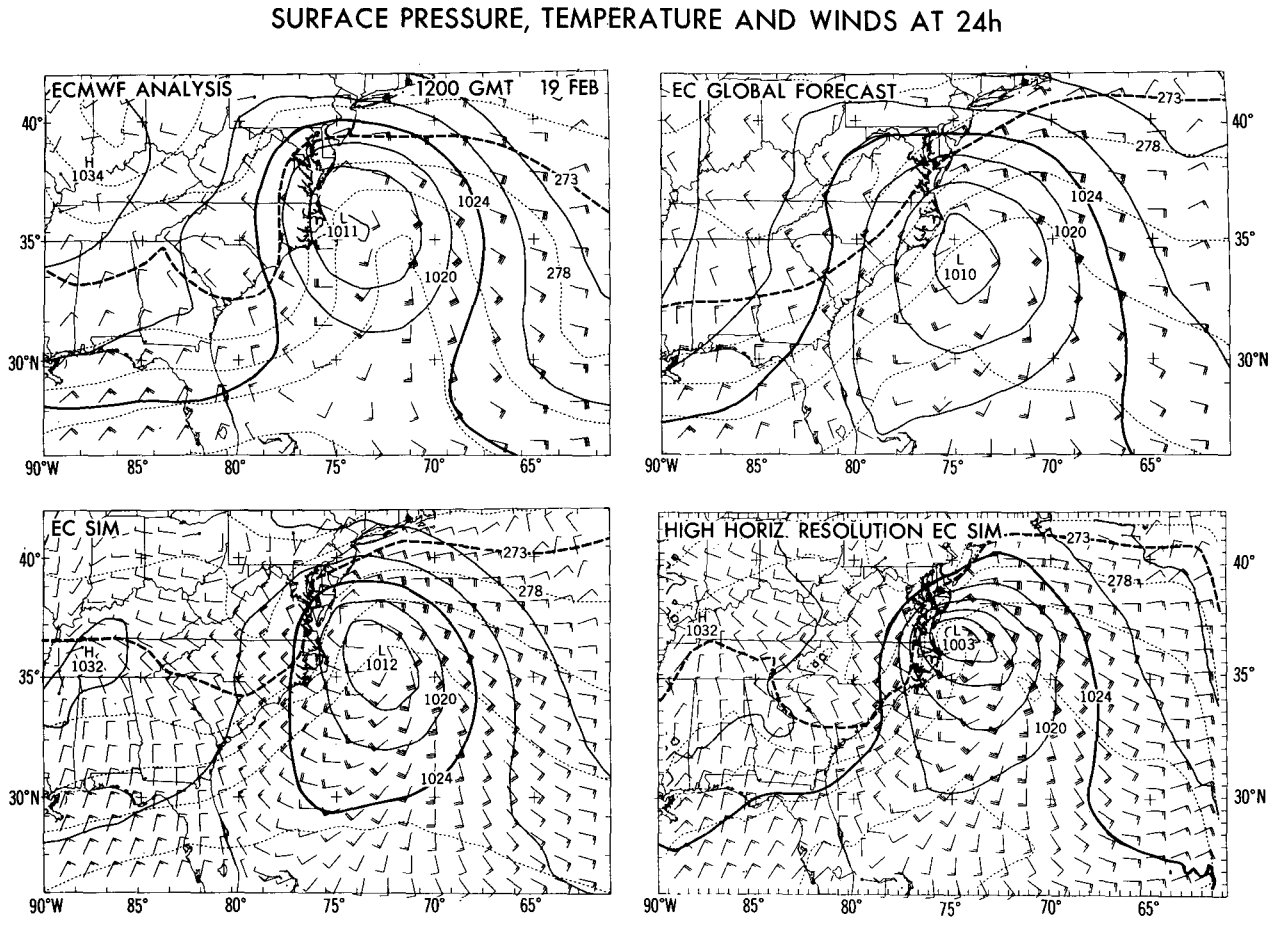

FIG. 21. Surface pressure, temperature, and winds at 24 h for ECMWF analysis (upper left), EC SPC forecast (upper right), EC SIM (lower left), and high horizontal resolution EC SIM (lower right). (Data in same format as Fig. 18 with 273 K and 1024 mb contours darkened).

to the control simulation except at the western boundary where the forecast was over 10 mb higher. The pressure of the surface low is about 2 mb higher for the forecast than for the simulation. The differences in the sea level pressure at 48 hours are of significantly greater magnitude than at 24 hours (up to 18 mb at the western boundary), with the surface low in the forecast deeper than the control.

The differences in 500 mb geopotential at 24 hours show generally good agreement between the forecast and the simulation but with greater ridging over the mid-Mississippi Valley. By 48 hours, the differences along the western boundary increased to 90 m, while lower forecasted heights are noted along the northern boundary. The short-wave trough located around 60°W is deeper in the forecast than the simulation. Since the forecast and simulation had identical initial conditions, differences which occur are due to the boundary conditions. A comparison of these differences with the differences between the spectral forecast and the analysis (Fig. 19) shows a strong similarity. Thus, by 48 hours the boundary conditions of the forecast which came from the spectral forecast had a considerable influence on the limited-area model forecast.

The 500 mb relative vorticity of the GF FOR is very similar to the control simulation at 24 hours, with only slightly larger values for the forecasted short wave located near Virginia (Fig. 23). These larger values result from the stronger ridging west of the short wave. By 48 hours, the differences become somewhat larger, with the short wave in the forecast becoming even stronger than in the simulation, in accordance with the deeper trough.

Differences between the EC FOR and the control simulation (GF SIM) for sea level pressure and 500 mb geopotential are shown in Fig. 24. The 24-hour forecasted sea level pressure is slightly deeper and is located east of the control simulation. Higher pressures are evident along the western boundary. By 48 hours, the surface low is several millibars deeper, while over the central U.S., differences greater than 6 mb occur, with the largest differences at the boundaries. The 500 mb geopotential shows a deeper trough over Virginia and higher heights over the Mississippi Valley at 24

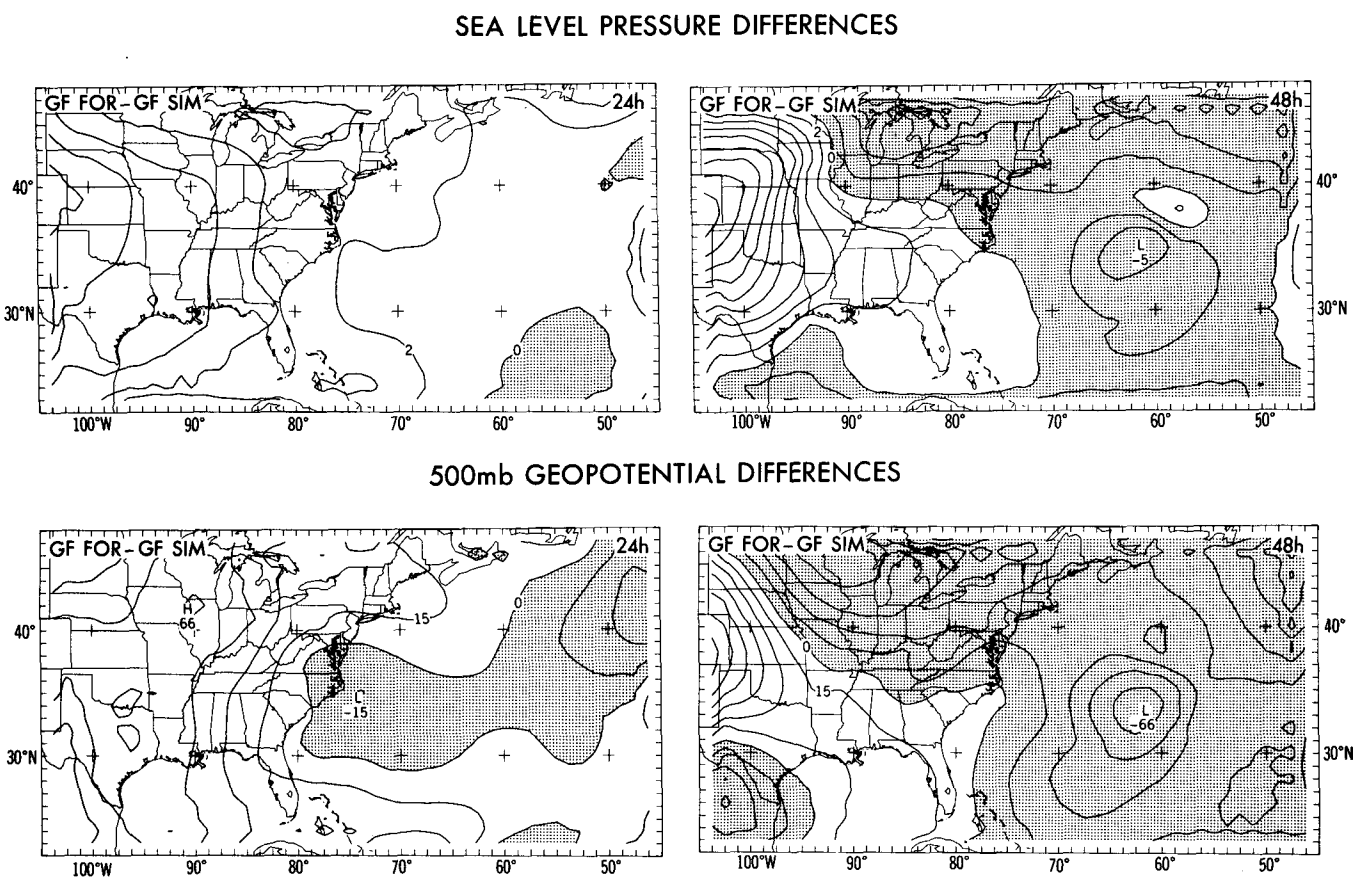

FIG. 22. Sea level pressure differences (top row, contour interval = 2 mb, negative values shaded) and 500 mb geopotential height differences (bottom row, contour interval = 15 m, negative values shaded) between GF FOR and control simulation at 24 h (left half) and 48 h (right half).

hours for the EC FOR than for the control simulation. Differences at 48 hours are larger, with the short-wave trough about 60 m deeper in the forecast. Although not shown, these differences are very similar to the differences of the EC SPC forecast (used as boundary conditions for EC FOR) and the GFDL analysis (used as boundary conditions for the control simulation). As with the GF FOR, the boundary-condition data has a strong influence on the limited-area forecast or simulation. This agrees with the findings of OMM and Orlanski (1984) on the importance of boundary data on limited-area forecasts.

A discrepancy exists for the GFDL case between the nonlinear normal mode (NLNM) initialized field in the global forecast and the noninitialized initial conditions for the limited-area forecast model. In order to test the impact of the NLNM initialization, a new simulation and forecast were run using the initialized GFDL data. The rms of the 500 mb geopotential height for these solutions are shown in Fig. 25. The upper graph shows the rms, with the GFDL/FGGE archived analysis as a reference. The limited-area simulation and forecast are those described in the text. The middle graph shows the same rms, with the reference analysis taken to be the NLNM initialized analysis. The limited-area simulation and forecast also use this initialized analysis. For a comparison, the lower graph shows the rms for the EC SPC forecast and the limited-area EC SIM and EC FOR with the ECMWF analysis as a reference.

The rms generally increases during the first 24 hours to a value of about 30 m and remains approximately constant to 48 hours. Note that this error is fairly small, consistent with the generally accurate development in the limited-area model. The initialized or uninitialized fields in the GF simulation and forecast do not show considerable difference. An interesting feature is the fact that in both cases with GFDL and ECMWF data, the limited-area model forecast mimics the rms of the global forecast to a considerable degree, as noted previously. In the ECMWF case (lower graph), the limited-area forecast and simulations are very close up to 24 hours; then the limited-area forecast rms increases to follow the global forecast up to 48 hours. One could have concluded that the initial conditions control the limited-area forecast during the first 24 hours, and boundary data from the global forecast affect the limited area forecast for times longer than 36 hours. This

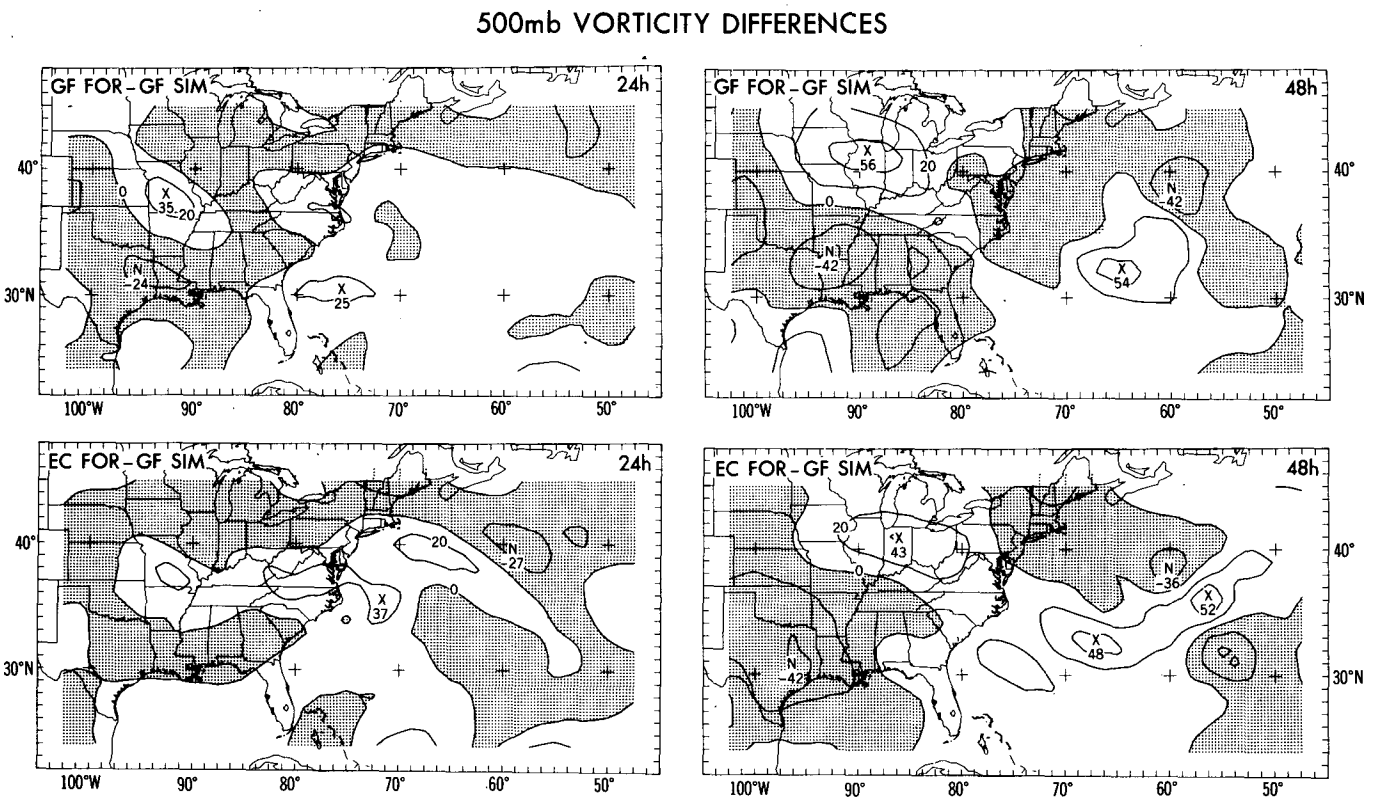

FIG. 23. Vertical component of 500 mb relative vorticity differences between GF FOR and control simulation (top row) and between EC FOR and control simulation (bottom row) at 24 h (left half) and 48 h (right half). Contour interval = 20×10^{-6} s^{-1}, negative values shaded.

clear picture, however, cannot be generalized because, as noted in the upper two graphs (especially the middle graph), the larger discrepancy of the global forecast at 24 hours compared with the simulation has been faithfully reproduced by the limited-area forecast, as well.

The 500 mb relative vorticity differences at 24 and 48 hours between the EC FOR and the control simulation (lower half of Fig. 23) are similar to the GF FOR differences, although they are slightly larger. The EC FOR short wave has larger relative vorticities than in the control simulation. Differences are also evident in the western portion of the domain, similar to those noted in the sea level pressure and 500 mb geopotential.

The evolution of the limited-area forecasted sea level pressure minima is shown in Fig. 26. At 24 hours, the lows in the simulations (see Fig. 12) are deeper than lows in the forecasts initialized with the same analysis. However, the forecasted lows became deeper by 36 hours. Thus the forecasted lows deepened more rapidly during this 12-hour period than the corresponding simulations. This is probably related to the stronger short wave in the forecasts than in the simulations.

10. Conclusions

The Presidents' Day snowstorm was successfully modeled using a nested limited-area model. Limited-area simulations and forecasts using ~150 km resolution model were successful in predicting the general development and movement of this storm. Some discrepancies were noted between the analyses and the model predictions for the intensity of upper-air features, especially during the first 24 hours. The most accurate prediction was obtained when a high-resolution model (~50 km) was used to simulate the development. The solution using this model not only accurately reproduced the position and intensity of the storm, but also some details of the mesoscale structure. However, the predicted precipitation was lacking north and west of the low.

The impact of using different analyses for initial conditions was less than the variability of the analyses themselves. Although significant differences were noted in the initial conditions, all simulations were remarkably similar for this case. This suggests that the limited-area model adjusted some of the initial differences to a state that was consistent with the model thermodynamics and dynamics. However, there were still differences in the simulations associated with differences in the initial conditions.

The development of the 500 mb relative vorticity maximum associated with the propagating short wave over the Ohio Valley was more consistent between model runs than with all the analyses. The model pre-

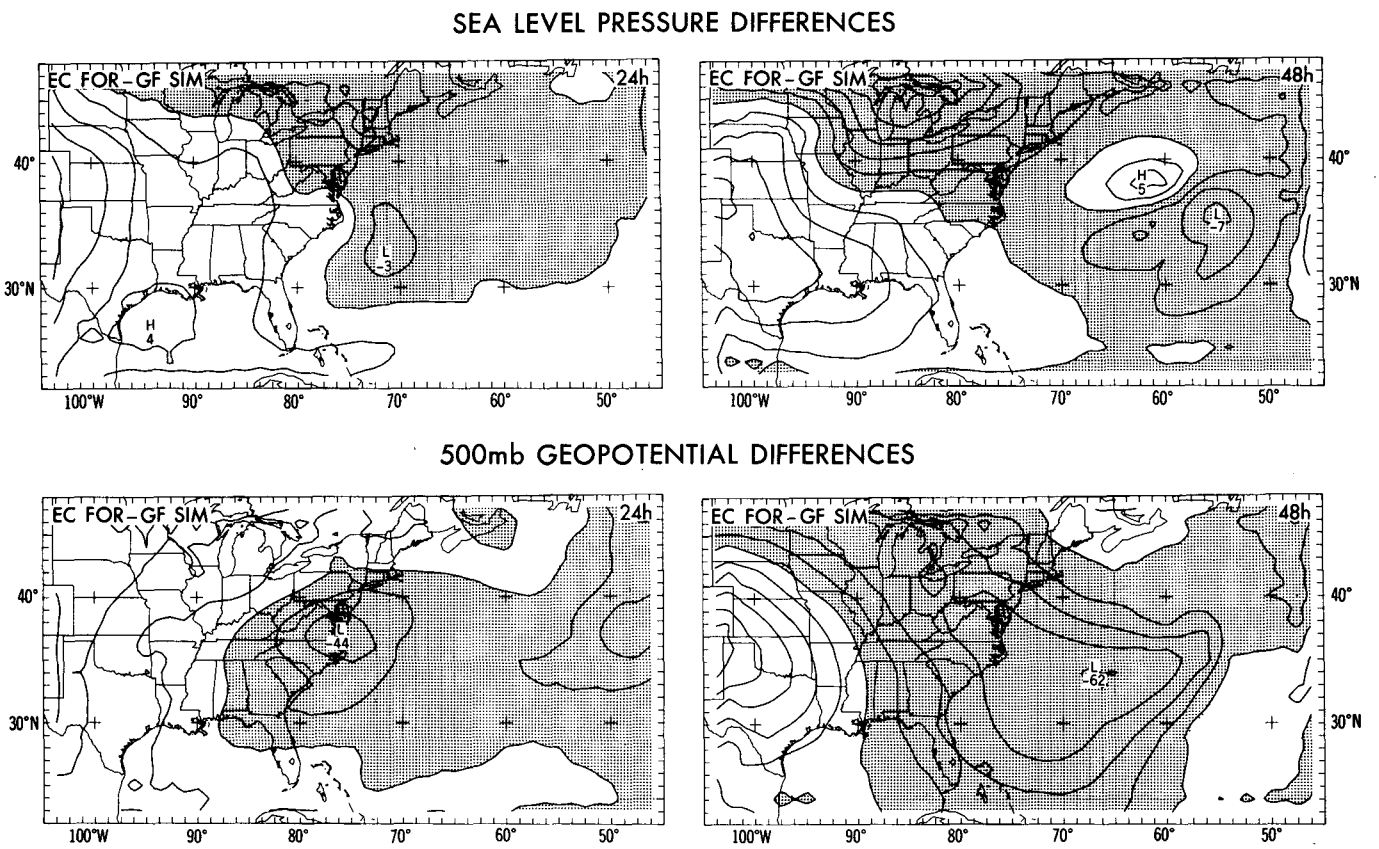

FIG. 24. Sea level pressure differences (top row, contour interval = 2 mb, negative values shaded) and 500 mb geopotential height differences (bottom row, contour interval = 15 m, negative values shaded) between EC FOR and control simulation at 24 h (left half) and 48 h (right half).

dicted nearly constant intensity of the short wave during the first 24 hours, followed by significant increases to around 36 hours and constant thereafter. The analyses generally indicated an increase in intensity to 24 hours, followed by decreases. Further investigation is needed to determine the cause of this discrepancy.

The importance of the horizontal diffusion used in the limited-area model was tested. In general, the results were as expected, with deeper development occurring when less horizontal diffusion was used. An interesting point is that the character and location of the development did not change significantly with changes in the horizontal diffusion. The intensity of the short wave remained nearly constant during the first 24 hours in all but the extreme cases, indicating that the diffusion was not a significant factor. Moreover, since the model successfully simulated the development of the coastal cyclone with a scale smaller than the upper trough, the effect of high diffusivity in preventing the intensification of the upper trough should be disregarded.

Latent heating was very important for the intensification of the low. However, the low did develop in a case without latent heat, implying that the initial low was forced by other mechanisms and that latent heating caused the storm to intensify much more rapidly. In addition, the release of latent heat aided the vertical development of the storm and caused significant changes in the 500 mb flow, in agreement with the findings of Atlas (1987).

The most significant improvement occurred in the simulation when the horizontal resolution was increased from 150 km to 50 km. The position and intensity of the surface low were much closer to reality, as indicated by the mesoscale analysis of Bosart (1981) (see Fig. 17) and through comparisons with satellite pictures (see Fig. 18a, b). It is important to use mesoscale analyses for verification, since global-scale analyses lack the detailed structure that the model predicts.

In general, the quality of the limited-area forecast was similar to the simulations. The position and intensity of the surface low, as well as the development of the short wave, were similar between the simulations and the forecasts.

The importance of the boundary conditions was demonstrated by using a global spectral forecast as boundary conditions for the limited-area model initialized with the same data as the corresponding simulations. The boundary conditions influenced the forecast as it progressed, primarily through advection and planetary wave propagation, into the limited-area

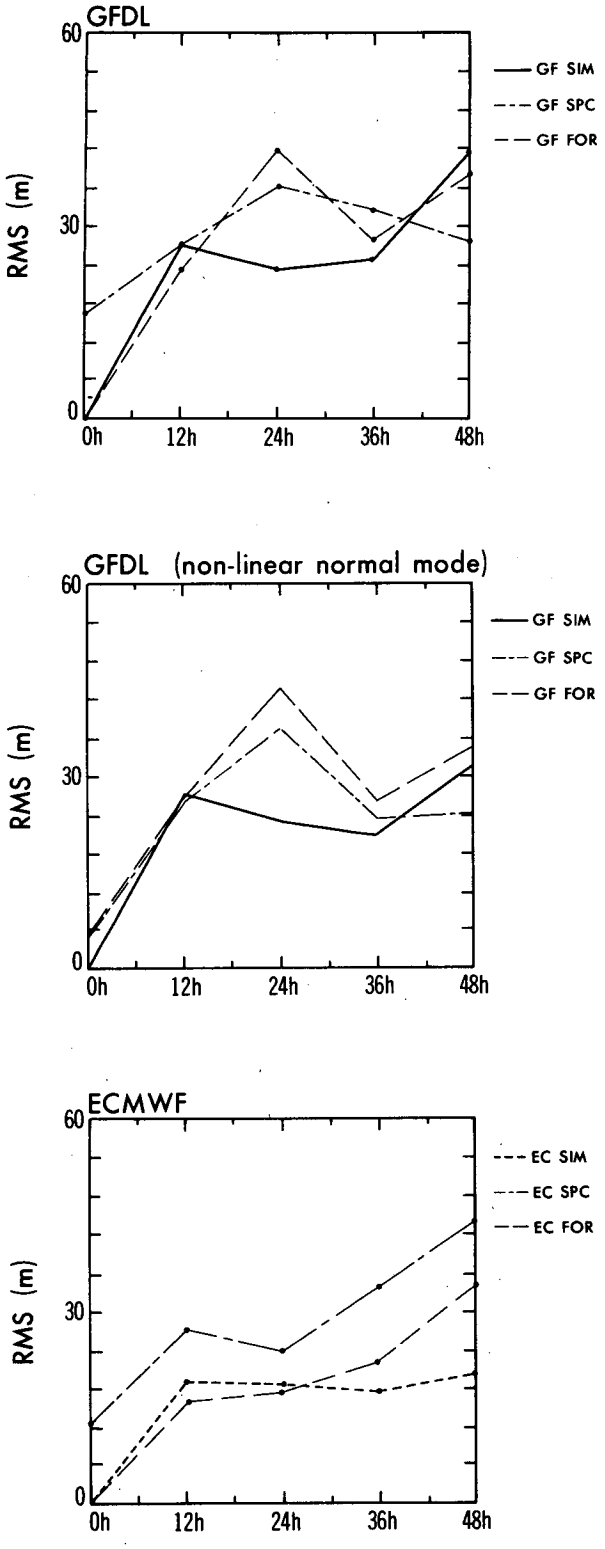

FIG. 25. The time evolution of the root-mean-square of the 500 mb geopotential height difference for indicated simulations and forecasts as compared to GFDL archive analysis (top panel), GFDL analysis after nonlinear normal mode initialization (middle panel), and ECMWF archive analysis (bottom panel). (For further information see text.)

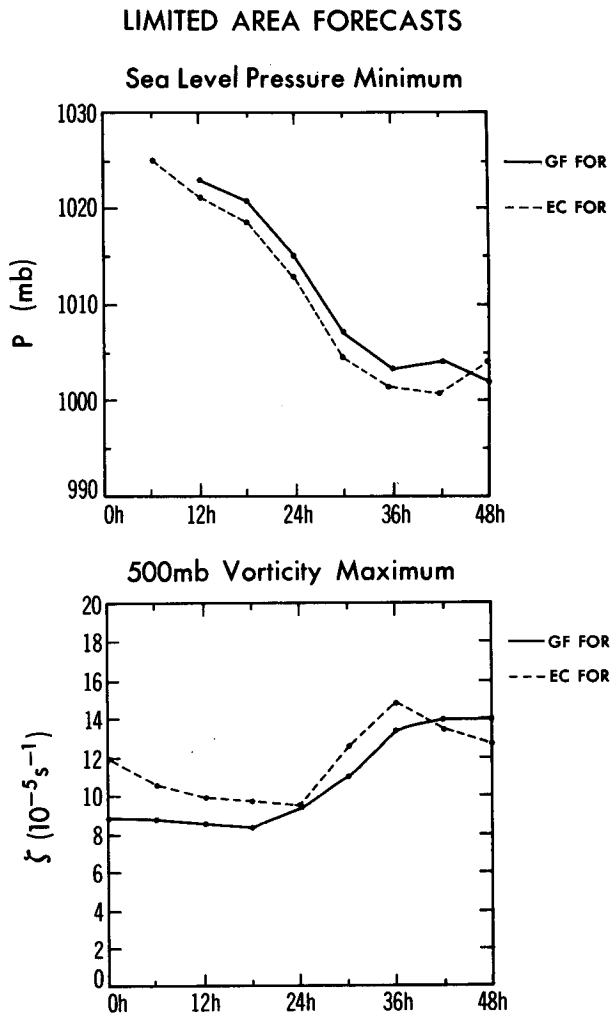

FIG. 26. Time evolution of the sea level pressure minimum (top panel) and 500 mb relative vorticity maximum (bottom panel) for GF FOR and EC FOR.

domain of values specified at the boundaries. Thus, the coarse global model forecast had a considerable influence on the limited-area forecast through the boundary conditions as time went on.

Acknowledgments. The authors wish to thank Dr. K. Miyakoda for his encouragement and suggestions in performing this research and for facilitating the use of the global spectral and limited-area models that are the basis of the nested system. We would also like to extend our appreciation to J. Sirutis and D. Miller for implementing the nested system, to W. Stern for consultation on the global spectral model, to J. Ploshay and R. White for assistance with data preparation, to L. Polinsky and J. Baum for their help with the analysis programs. Dr. R. Atlas kindly provided the NMC and GLAS datasets.

We would also like to thank Dr. K. Miyakoda, F. Sanders, L. Uccellini, and B. Ross for their comments

on the manuscript, along with the GFDL drafting department and Mr. J. Conner for their assistance in preparing the figures.

APPENDIX[5]

Description of Models Used

a. The nested model system

The nested global, limited-area model used in this study consists of a global spectral model or analysis, providing boundary conditions to a limited-area model of enhanced resolution in a one-way nesting procedure. Both the global spectral and the limited-area models are initialized from the same set of analyzed observational data, and the simulations are performed for a 48-hour period.

b. The global spectral model

The large-scale model chosen for these purposes is the GFDL spectral model of Gordon and Stern (1982). The particular R30L09 version utilized represents scalar prognostic variables as an expanded series of spherical harmonics, with rhombodial truncation at wavenumber 30. Nonlinear dynamical terms and those describing physical processes are transferred to a global Gaussian grid for evaluation. The grid, which is of appropriate resolution for the truncation wavenumber 30, has 96 equispaced points around each of the 80 latitude circles, for a nominal grid intervals of 3.75° longitude and 2.25° latitude. The domain is defined in the vertical by nine sigma levels, spaced so as to resolve the planetary boundary layer, troposphere, and stratosphere equally well. The surface topography is interpolated to the 96 by 80 Gaussian transform grid from Scripps Institution Oceanography 1° by 1° latitude by longitude dataset and is then synthesized to the R30 spectral domain. The atmospheric lid is defined at 0 mb.

The physical processes incorporated in these spectral runs, including a GFDL physics package, consist of linear fourth-order horizontal diffusion of temperature, momentum, and moisture; bulk aerodynamic drag laws to describe surface boundary layer fluxes, with constant surface drag coefficients defined over the land and sea independently; Prandtl mixing-length theory to determine the vertical diffusion of momentum and water vapor in the planetary boundary layer; a vertical heat transport and precipitation scheme consisting of large-scale condensation within supersaturated layers, and moist convective adjustment in conditionally unstable layers exceeding 80% saturation, with precipitation allowed to accumulate as either rain or snow; a soil moisture state determined by a balance between evaporation, precipitation and snow melt which in turn determines the extent of surface evaporation; a diurnally varying, latitudinally dependent formulation of zenith angles for determination of incoming solar radiation; specification of albedo as a function of surface type (land, snow, ocean, or sea ice) and zenith angle; determination of surface temperature from a balance of short-wave, long-wave, sensible heat, and latent heat fluxes and, when present, heat conduction through sea-ice; and use of radiative transfer algorithms, redetermined at 12-hour intervals, for calculation of long- and short-wave heat fluxes. For these radiative balances, distributions of the important atmospheric constituents ozone, water vapor, cloudiness, and carbon dioxide are specified from climatological, zonally averaged fields: the first three of these varying seasonally and the latter being fixed annually.

c. The limited area model

The nested model chosen for the experiments is a limited-area version of the HIBU[6] model (Janjic, 1977; Mesinger, 1977, 1981; Mesinger and Strickler, 1982) originally developed at the Federal Hydrological Institute and Belgrade University, Yugoslavia. The subgrid parameterization and physics are from the GFDL experimental prediction group at GFDL, Princeton. (The physics implementation in the limited area model was done by J. Sirutis of the experimental prediction group.) It is a grid-point model on a staggered Arakawa type-E latitude–longitude grid (Arakawa, 1972), with mass and momentum quantities being defined at alternate points of the mesh.

There are nine sigma levels in the vertical, which are defined similarly but not identically to those of the GFDL spectral model previously described. The surface topography is interpolated to the limited-area grid from a high-resolution set of elevations. Around the perimeter of the limited-area domain, however, the topography is replaced by the more coarsely resolved topography of the spectral model, with a smooth transition zone existing in the four outermost grid rows of the limited-area border region. The atmospheric lid is defined at 1.98 mb, for which value a surface pressure of 1013.25 mb will yield exact correspondence in space between the integer sigma levels of the limited-area and spectral models.

The conservational properties of this model would seemingly make it an excellent choice for limited-area utilization. Its fourth-order horizontal advection schemes conserve enstrophy for the rotational component of the wind, conserve kinetic energy for the rotational and divergent components of the wind, and conserve total energy and moisture within any closed domain. These properties enable the advection terms to be calculated only once every two timesteps of the explicit, two-time level Heun scheme used for the for-

[5] Contributed by D. Miller.

[6] Federal Hydrometeorological Institute and Belgrade University.

ward integrations, resulting in improved computational usage without diminishing the accuracy of the solutions. In fact, the fourth-order nature of these schemes has been shown to yield improved simulations of the speed of synoptic disturbances, compared to analogous second-order schemes.

With its inclusion of finely resolved, and at times steep, topography, the model employs a formulation of the pressure gradient and Coriolis force terms which would avoid a possible, spurious height-staggering of these two terms on sharply inclined sigma surfaces.

Damping of divergence is performed during the first nine hours of the limited-area simulation to diminish possible noises introduced by imbalances in the initial fields. A treatment of the divergence term in the continuity equation which handles gravity waves via propagation from their point of generation to neighboring points only suppresses the false growth of two-grid-interval noise. Because of this and other conservation properties of the model, horizontal diffusion is considered to be of relatively minor importance, particularly in a simulation of only a few days (Mesinger, 1981). Nevertheless, horizontal diffusion of momentum, temperature, and moisture is determined at the same time intervals as those used for the horizontal advection terms, with a coefficient chosen for all the diffusion terms which, when normalized to the current grid, yields a value of about 4×10^5 m^2 s^{-1}.

The "physics" included in the model is that of the GFDL E2 package. (The E2 physics was developed by K. Miyakoda and J. Sirutis of the GFDL Experimental prediction group.) As in the spectral model physics, Prandtl mixing-length theory is used for determining vertical diffusion in the planetary boundary layer; vertical heat transport is achieved via dry convective adjustment; a combination of large-scale condensation and moist convective adjustment at an 80% criterion is used for parameterizing precipitation, snow melt, and evaporation. However, surface drag is formulated via a Richardson number-dependent Monin-Obukov scheme, and the slightly more sophisticated Fels-Schwarzkopf parameterizations are used for determining radiative heat fluxes. Solar zenith angle is calculated to the day for determining insolation and albedo as functions of latitude, but diurnal variations of the sun's azimuthal angle are not incorporated.

d. Time-dependent boundary conditions

After each 20 minute timestep of the spectral solution, boundary conditions are fed to the limited area model. Updated fields of the prognostic variables (U, V, T, Q, lnP^*) are transformed from their spectral representations to the 96 by 80 global Gaussian grid in the vicinity of the nested domains' perimeter. They are then horizontally interpolated via a four-point scheme, and vertically interpolated via cubic splines, to the outermost mass and momentum grid points of the limited-area domain grid. A similar procedure is done when the boundary conditions come from an analysis. Finally, a linear interpolation is done in time, and these values are input as boundary conditions at every timestep of the 48-hour solution.

A transition zone is also established for the treatment of the horizontal advection and diffusion terms. At the row of points one in from the border, a buffer line is established where fields are determined via a four-point spatial averaging of the border points and at the next interior line of grid points. Then, immediately inside this buffer line, a four-point Lagrangian-type upstream horizontal advection scheme is used at the next three grid lines. The coefficient of horizontal diffusion is set 10 times higher than in the domains' interior at the next five inner grid rows.

At the outermost grid points, the values of U, V, T, Q and P^* are all prescribed from the boundary conditions, except for the tangential components of momentum which, for conditions of outflow, are extrapolated from the model's interior.

REFERENCES

Anthes, R. A., 1983: A review of regional models of the atmosphere in middle latitudes. *Mon. Wea. Rev.*, **111**, 1306–1335.

——, Y.-H. Kuo, S. G. Benjamin and Y.-F. Li, 1982: The evolution of the mesoscale environment of severe local storms: Preliminary modeling results. *Mon. Wea. Rev.*, **110**, 1187–1213.

Arakawa, A., 1972: Design of the UCLA general circulation model. Numerical Simulation of Weather and Climate, Dept. of Meteorology, UCLA, Tech. Rep. 7, 116 pp.

Atlas, R., 1987: The role of oceanic fluxes and initial data in the numerical prediction of an intense coastal storm. *Dyn. Atmos. Oceans*, **10**, 359–388.

Baker, W., 1983: Objective analysis and assimilation of observational data from FGGE. *Mon. Wea. Rev.*, **111**, 328–342.

Bengtsson, L., M. Kanamitsu, P. Kallberg and S. Uppalla, 1982: FGGE 4-dimensional data assimilation at ECMWF. *Bull. Amer. Meteor. Soc.*, **63**, 29–43.

Bosart, L. F., 1981: The Presidents' Day snowstorm of 18–19 February 1979: A subsynoptic-scale event. *Mon. Wea. Rev.*, **109**, 1542–1566.

——, and S. C. Lin, 1984: A diagnostic analysis of the Presidents' Day storm of February 1979. *Mon. Wea. Rev.*, **112**, 2148–2177.

Gordon, C. T., and W. F. Stern, 1982: A description of the GFDL global spectral model. *Mon. Wea. Rev.*, **110**, 625–644.

Janjic, Z. I., 1977: Pressure gradient force and advection scheme used for forecasting with steep and small-scale topography. *Contrib. Atmos. Phys.*, **50**, 186–199.

Koch, S. E., W. C. Skillman, P. J. Kocin, P. J. Wetzel, K. F. Brill, D. A. Keyser and M. C. McCumber, 1985: Synoptic-scale forecast skill and systematic errors in the MASS 2.0 model. *Mon. Wea. Rev.*, **113**, 1714–1737.

Kocin, P. J., L. W. Uccellini, J. W. Zack and M. L. Kaplan, 1985: A mesoscale numerical forecast of an intense convective snowburst along the east coast. *Bull. Amer. Meteor. Soc.*, **66**, 1412–1424.

Kung, E. C., and H. Tanaka, 1983: Energetics analysis of the global circulation during the special observation periods of FGGE. *J. Atmos. Sci.*, **40**, 2575–2592.

Lau, Ngar-Cheung, 1985: Publication of circulation statistics based on FGGE level III-B analyses produced by GFDL and ECMWF. *Bull. Amer. Meteor. Soc.*, **66**, 1293–1301.

McPherson, R. D., K. H. Bergman, R. E. Kistler, G. E. Rasch and

D. S. Gordon, 1979: The NMC operational global data assimilation system. *Mon. Wea. Rev.*, **107**, 1445–1461.

Mesinger, F., 1977: Forward-backward scheme, and its use in a limited area model. *Contrib. Atmos. Phys.*, **50**, 200–210.

——, 1981: Horizontal advection schemes of a staggered grid—An enstrophy and energy-conserving model. *Mon. Wea. Rev.*, **109**, 467–478.

——, and R. F. Strickler, 1982: Effect of mountains on Genoa cyclogenesis. *J. Meteor. Soc. Japan*, **60**, 326–338.

Orlanski, I., 1984: Lectures on the dynamics of mesoscale weather systems. Advanced Study Program, NCAR.

——, D. Miller, and K. Miyakoda, 1983: The impact of initialization analyses in the forecasting of precipitation patterns. *Papers presented at the Workshop on Very Short-Range Forecasting Systems-Research Aspects*, 15–17 August 1983, Boulder, Short- and Medium-Range Weather Prediction Research Publication Series, No. 5, World Meteor. Organization, 59–62.

——, B. B. Ross, L. J. Polinsky and R. W. Shaginaw, 1985: Advances in the theory of atmospheric fronts. *Adv. Geophys.*, **28B**, 223–252.

Ross, B. B., 1987: The role of low-level convergence and latent heating in a simulation of observed squall-line formation. *Mon. Wea. Rev.*, in press.

Stern, W. F., and J. J. Ploshay, 1983: An assessment of GFDL's continuous data assimilation system used for processing FGGE data. *Preprints, 6th Conf. on Numerical Weather Prediction*, Omaha, Amer. Meteor. Soc., 90–95.

——, and ——, 1987: The post-FGGE data assimilation system at GFDL. *Global Weather Experiment Newsletter*, **17**, 5–13. BASC, JH810, National Academy of Sciences/NRC, Washington, D.C.

Tuleya, R. E., M. A. Bender and Y. Kurihara, 1984: A simulation study of the landfall of tropical cyclones using a moveable nested-mesh model. *Mon. Wea. Rev.*, **112**, 124–136.

Uccellini, L. W., D. Keyser, K. F. Brill and C. H. Wash, 1985: The Presidents' Day cyclone of 18–19 February 1979: Influence of upstream trough amplification and associated tropopause folding on rapid cyclogenesis. *Mon. Wea. Rev.*, **113**, 962–988.

——, P. J. Kocin, R. A. Peterson, C. H. Wash and K. F. Brill, 1984: The Presidents' Day cyclone of 18–19 February 1979: Synoptic overview and analysis of the subtropical jet streak influencing the precyclogenetic period. *Mon. Wea. Rev.*, **112**, 31–55.

——, R. A. Petersen, P. J. Kocin, M. J. Kaplan, J. W. Zack and V. C. Wong, 1983: Mesoscale numerical simulations of the Presidents' Day cyclone: Impact of sensible and latent heating on the pre-cyclogenetic environment. *Preprint, 6th Conf. Numerical Weather Prediction*, Omaha, Am. Meteor. Soc., 45–52.

Weisman, M. L., and J. B. Klemp, 1982: The dependence of numerically simulated convective storms on vertical wind shear and buoyancy. *Mon. Wea. Rev.*, **110**, 504–520.